

ENERGY MINIMIZATION OF 2D INCOMMENSURATE HETEROSTRUCTURES

PAUL CAZEAUX*, MITCHELL LUSKIN†, AND DANIEL MASSATT†

Abstract. We derive and analyze a novel approach for modeling and computing the mechanical relaxation of incommensurate 2D heterostructures. Our approach parametrizes the relaxation pattern by the compact local configuration space rather than real space, thus bypassing the need for the standard supercell approximation and giving a true aperiodic atomistic configuration. Our model extends the computationally accessible regime of weakly coupled bilayers with similar orientations or lattice spacing, for example materials with a small relative twist where the widely studied large-scale moiré patterns arise [21, 33]. Our model also makes possible the simulation of multi-layers for which no interlayer empirical atomistic potential exists, such as those composed of MoS₂ layers, and more generally makes possible the simulation of the relaxation of multi-layer heterostructures for which a planar moiré pattern does not exist.

Key words. 2D materials, heterostructures, ripples, incommensurability, atomistic relaxation, Frenkel-Kontorova

AMS subject classifications. 65Z05, 70C20, 74E15, 70G75

Introduction. Two-dimensional (2D) crystals have been intensely investigated both experimentally and theoretically since graphene was exfoliated from graphite [26]. Graphene has been shown to have exceptional mechanical strength and electrical conductivity, but its lack of a band gap limits its technological application [11]. Many other two-dimensional crystals such as the insulator h-BN and semiconductor MoS₂ have since been experimentally realized. More recently, physicists have developed the ability to stack one layer on another with a twist angle controlled to the scale of .1 degree with the goal of creating 2D materials with desired electronic, optical, and mechanical properties [19].

Although each layer is crystalline and has a periodic structure when isolated, the ground state mechanical configuration of weakly coupled multi-layer 2D systems is generally no longer periodic when the individual layers have incommensurate lattice constants such as when graphene is stacked on MoS₂ or when one 2D crystal such as graphene or MoS₂ is stacked and rotated on a like layer [6, 25]. Moreover, the periodic configuration of each layer is no longer a mechanical ground state when so stacked and the relaxation creates large scale moiré patterns that dramatically affect electronic properties.

To study mechanical relaxation for a particular twist angle or set of lattice constants, previous works have approximated the incommensurate system using an artificial strain or twist to force the system to be periodic on a supercell. In [31], for example, the relaxation of bilayer graphene on supercells was studied using interatomic potentials, REBO for intralayer coupling and Kolmogorov-Crespi for interlayer coupling. This approach is no longer feasible for small twist angles because the length scale of the supercell approximation scales inversely to the twist angle, in addition to restricting the set of configurations which can be probed [29].

Other previous works have proposed or derived continuum models on moiré cells or supercells by imposing *a priori* periodic boundary conditions, bypassing the need to strain the system into periodicity as for atomistic models. It is, however, not clear how

*Department of Mathematics, University of Kansas, Lawrence, KS 66049 (pcazeaux@ku.edu)

†School of Mathematics, University of Minnesota, Minneapolis, MN 55455 (luskin@umn.edu, massatt067@umn.edu)

to rigorously link such periodic continuum deformations with the underlying aperiodic atomistic configurations for incommensurate heterostructures. In [16], a continuum elastic model was used for intralayer interactions while a generalized stacking fault energy (GSFE) for bilayer graphene was used to capture interlayer interactions, and in [34] intralayer interactions in bilayer graphene were also modeled by continuum elasticity and the intralayer interactions were modeled by a disregistry energy calculated from the Kolmogorov-Crespi interlayer atomistic potential. A continuum model for the approximation of an incommensurate deformable lattice coupled to a rigid substrate was derived in [17].

This paper presents a new approach to modeling and computing the mechanical relaxation pattern of weakly coupled incommensurate bilayers by parametrizing the relaxation pattern by local configuration space rather than real space. This concept of *hull*, a compact parametrization of all possible local environments, was originally introduced for the study of quantum electronic models of general aperiodic solids [2, 3, 28] and recently extended to incommensurately stacked multi-layer assemblies [6, 25]. The local configuration (disregistry) is given by the projection of the atomic positions of each layer onto the unit cell of the other layer and is a compact representation of the local environment. Our method is thus not limited by a supercell approximation and provides the true representation of aperiodic atomistic configurations. The 2D theory presented in this paper was explored in a 1D model in [12] where a rigorous proof using Aubry-Mather theory is given that energy minimizers can be parameterized by local configuration.

We derive a Cauchy-Born energy density for the intralayer interactions and a generalized stacking fault energy for the interlayer interactions, and we then derive the continuum elastic model by using the ergodicity of the local configurations with respect to the translation group. The use of the GSFE allows the modeling of interlayer interactions in 2D heterostructures for materials for which interatomic potentials are not available, such as MoS₂, and can be expected to be more accurate than interatomic potentials since the GSFE is fit directly from DFT calculations [10, 36]. An application of our approach to small angle twisted bilayer graphene and MoS₂ is given in [10].

For the particular case of bilayer heterostructures, our model gives a well-posed variational problem for the continuum displacement field on the periodic moiré domain. We then represent the actual atomistic positions by sampling the continuum displacement field at the atomistic positions of the unrelaxed incommensurate heterostructure to give the relaxed aperiodic atomistic configuration. This provides us with the missing link between the atomistic picture and existing continuum bilayer models [16]. These relaxed atomistic configurations can then be used to compute diffraction patterns [33] or electronic density and transport properties [6, 25]. Previous approaches to compute atomistic configurations in relaxed heterostructures have been limited by the size of the supercell approximation at small twist angles [31, 34]. For incommensurate multi-layer heterostructures, our model more generally gives a variational problem for the relaxation of incommensurate multi-layer heterostructures for which the continuum model is not periodic on any two-dimensional domain.

In section 1, we describe the geometry of multi-layered structures, and in section 2, we present our formulation for the continuum disregistry of both unrelaxed and relaxed incommensurate layers by interpolation from the atomistic disregistry. In section 3, we derive the continuum elastic model for the relaxation of weakly coupled incommensurate layers, and in section 4 we give an analysis of our elastic model for bilayers. In section 5, we present our numerical approximation and give computational

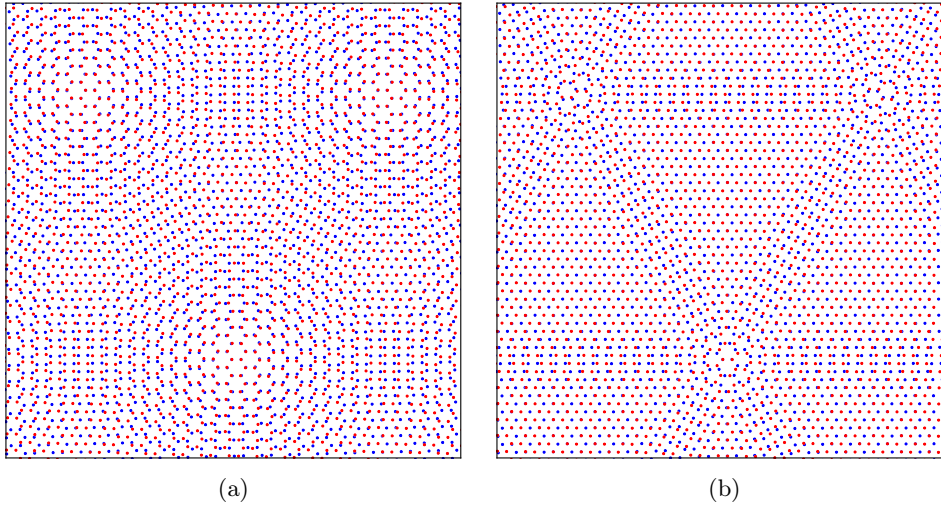


Fig. 1: Illustration of the collective, registry-driven relaxation of atomic moiré patterns. (a) Unrelaxed atomic positions of G/G bilayer with a 3° twist angle. (b) Domain structure after relaxation. The inter-layer interaction forces are enhanced by $\times 100$ for visualization purpose.

results for twisted bilayers.

1. Geometry of multi-layered structures. Two dimensional heterostructures are vertical stacks of a few crystalline monolayers, which typically have different periodicities. Due to the weak van der Waals nature of the interactions between layers, little relaxation usually take place as the layers are mechanically stacked on top of each other, rather each layer essentially keeps the crystalline structure it possesses as an isolated monolayer. The resulting assembly is in general an aperiodic system with long-range order. This order is usually most noticeable when the lattices have close, but slightly different spacing and/or orientation, creating large scale moiré patterns. In this case, an ordered, locally collective relaxation motion of atoms can take place as the layers maximize the area of energetically favorable stacking (See Figure 1).

1.1. Notations. A systematic model of the relaxation of such heterostructures starts by a rigorous depiction and parameterization of the particular geometry of unrelaxed ideal multilayered structures, which will serve as a reference configuration in the elastic modeling of the relaxation phenomenon. We summarize in this section the findings of [6], where the geometry of these perfect multilayer structures was analyzed and discussed in detail.

We consider a 3-dimensional system of p parallel 2-dimensional periodic atomic layers, denoted $\mathcal{L}_j \subset \mathbb{R}^3$, $j = 1 \dots p$. We denote by

- $(\mathbf{e}_1, \mathbf{e}_2, \mathbf{e}_3)$ an orthonormal basis of the physical space such that each layer is perpendicular to \mathbf{e}_3 ; from now on, points in physical space will be identified with their cartesian coordinates $(x, y, z)^T$ associated with this basis;
- h_j the third coordinate, or height of the center of layer j . We assume that $0 = h_1 < h_2 < \dots < h_p$ without loss of generality;
- \mathcal{R}_j , $j = 1 \dots p$ the 2-dimensional periodic lattice of layer j ;

- E_j the matrix in $\mathbb{R}^{2 \times 2}$ whose columns form a basis generating the layer \mathcal{R}_j , that is,

$$(1.1) \quad \mathcal{R}_j := E_j \mathbb{Z}^2 \subset \mathbb{R}^2;$$

- $\Gamma_j := \mathbb{R}^2 / \mathcal{R}_j$ the quotient of \mathbb{R}^2 by the discrete lattice \mathcal{R}_j , which has the topology of a 2-dimensional torus and can be canonically identified with the periodic unit cell $\hat{\Gamma}_j := E_j[-1/2, 1/2]^2$ of layer j .

REMARK 1.1. *These definitions give an essential description of the crystal structure. However, it is always possible to describe even a simple crystal as a multilattice crystal with a unit cell containing more than one atom. Such non-essential descriptions allow for translation symmetry-breaking deformations, including phase transformations, which are known to occur in 2D materials, e.g., in transition metal dichalcogenides under stress.*

1.2. Shifts and disregistry: the hull. The above definitions provide a description of each layer of the vertical stack in an unperturbed state at a fixed height and at a fixed rotation angle. However, they do not account for the possibility of the layers sliding with respect to each other. This additional degree of freedom is very important as it allows one to parameterize the ensemble of all possible configurations which can be observed for a lattice site within the stack. The ensemble of possible configurations can be identified with the so-called *hull* [2, 3], introduced previously in the study of the electronic structure of aperiodic materials. The idea behind the hull is to picture the position of observation from any point in the layer plane as the origin of coordinates, and the local environment as the neighboring atoms¹. This is particularly relevant to model the elastic relaxation of the stack, since as we shall see in Section 3.1, the local environment of an atom typically determines its energetics due to the locality of bonding.

In the context of multilayer stacks, the hull was rigorously identified in the earlier paper [6]. Since each layer is perfectly periodic in this reference, unrelaxed state, the position of all atoms in layer j is fully identified by the knowledge of a single vector γ_j in its periodic unit cell Γ_j , which we call a *disregistry*. The vertices of this layer j then form the shifted lattice $\gamma_j + \mathcal{R}_j$. The overall configuration can thus be uniquely parameterized as an element $\omega = (\gamma_1, \dots, \gamma_p)$ of the cartesian product:

$$(1.2) \quad \Omega = \Gamma_1 \times \dots \times \Gamma_p.$$

We present in Figure 2 a one-dimensional example where an arbitrary configuration is labeled by an element of Ω . Finally, the change of coordinate origin (our viewpoint) is naturally associated with the action of the group \mathbb{R}^2 on Ω by translations \mathbf{T} that are parallel to the layers:

$$(1.3) \quad \text{For } \mathbf{a} \in \mathbb{R}^2, \quad \mathbf{T}_{\mathbf{a}} : \begin{cases} \Omega \rightarrow \Omega, \\ (\gamma_1, \dots, \gamma_p) \rightarrow (\gamma_1 + \mathbf{a}, \dots, \gamma_p + \mathbf{a}). \end{cases}$$

¹A configuration is rigorously defined as the position of all atoms in the system relative to the origin, given an arbitrary translation of the system corresponding to a change of viewpoint, typically encoded as a Radon measure in $\mathfrak{M}(\mathbb{R}^3)$. Formally, the hull is a dynamical system $(\Omega, \mathbb{R}^2, \mathbf{T})$ where Ω is the closure of the orbit of the atomic distribution generated by the atoms of all p layers under the action of \mathbb{R}^2 through \mathbf{T} . Note that the group of translations $\mathbf{T}_{\mathbf{a}}$ with $\mathbf{a} \in \mathbb{R}^2$ acts on the space of compactly supported continuous functions $\mathcal{C}_c(\mathbb{R}^3)$ naturally through $\mathbf{T}_{\mathbf{a}}f(\mathbf{x}) = f(\mathbf{x} - \mathbf{a})$, and thus on the space of Radon measures $\mathfrak{M}(\mathbb{R}^3)$ through $\mathbf{T}_{\mathbf{a}}\mu(f) = \mu(\mathbf{T}_{-\mathbf{a}}f)$.

1. \mathbb{P} is invariant by the translation group \mathbb{R}^2 ;
2. the dynamical system $(\Omega, \mathbb{R}^2, \mathbb{T}, \mathbb{P})$ is uniquely ergodic if and only if the lattices $\mathcal{R}_1, \dots, \mathcal{R}_p$ are incommensurate. In this case, we have the Birkhoff property: for any $f \in C(\Omega)$ and $\omega \in \Omega$,

$$(1.5) \quad \lim_{r \rightarrow \infty} \frac{1}{|B_r|} \int_{B_r} f(\mathbb{T}_{-\mathbf{a}}\omega) d\mathbf{a} = \int_{\Omega} f d\mathbb{P},$$

where B_r is the ball of radius r centered at zero.

Note that there are arrangements which are neither periodic, nor incommensurate (for example, two identical and aligned layers stacked on a third twisted one). In such cases, it is possible to find an appropriate decomposition of the lattices such that a smaller space of configurations Ω can be constructed and the corresponding hull is ergodic. We will not detail this procedure, and instead concentrate our efforts on the generic incommensurate case presented above.

2. Elastic models for incommensurate layers.

2.1. Continuum kinematics. Let us first discuss the case of continuous deformation fields relevant to a continuum (e.g., plate) modeling of the elastic behavior before turning to the case of atomistic models later on in Section 2.3. Our main assumption in this paper is that there is a one-to-one smooth correspondance between the displacement of any point belonging to one of the layers and their initial configuration through the elastic relaxation process. We thus introduce a set of modulation fields with respect to the reference (unrelaxed) positions, which takes the form of j functions

$$(2.1) \quad \mathbf{u}_j \in C(\Omega, \mathbb{R}^2), \quad 1 \leq j \leq p,$$

indexing the displacement of an arbitrary point in each of the layer planes depending on its configuration. The fields \mathbf{u}_j have the periodicity of the (dp) -torus Ω and represent the *structural modulation* of each layer due to the presence of the others.

REMARK 2.1. *In the case of multi-lattices such as graphene, a rigorous treatment should include additionally shift fields allowing for independent motion of the sublattices [30]. For the sake of simplicity, we neglect this complication in this paper.*

REMARK 2.2. *The key assumption behind the hull description is that there exists a one-to-one correspondance between the configuration of an atom and its modulated position in the relaxed configuration. This is a reasonable assumption due to the inherent stability of the individual lattices of the layers and the weakness of the Van der Waals interactions between the layers. In 1D, this is known to be strictly true for the Frenkel-Kontorova model for atomic chains with strictly convex nearest-neighbor atomic potentials sitting in an external incommensurate potential [1].*

Correspondance between real-space and hull descriptions. For any given configuration $\omega = (\gamma_1, \dots, \gamma_p) \in \Omega$, in the j -th layer, the real-space displacement, \mathbf{U}_j^ω , and deformation, \mathbf{Y}_j^ω , fields evaluated at any point $\mathbf{x} \in \mathbb{R}^2$ can be obtained from the modulation field \mathbf{u}_j by the formulae

$$(2.2) \quad \mathbf{U}_j^\omega(\mathbf{x}) = \mathbf{u}_j(\mathbb{T}_{-\mathbf{x}}\omega), \quad \mathbf{Y}_j^\omega(\mathbf{x}) = \mathbf{x} + \mathbf{u}_j(\mathbb{T}_{-\mathbf{x}}\omega).$$

This representation allows us in particular to rewrite the strain as a directional derivative in the hull framework. Given the action of the translation on the hull (1.3), it is

appropriate to introduce the spatial derivative on Ω as the operation

$$(2.3) \quad \nabla_{\mathbf{x}} := - \sum_{j=1}^p \nabla_{\gamma_j}.$$

Thus the local deformation for layer j in the configuration ω can be computed directly in the hull representation as $\mathbf{I} + \nabla_{\mathbf{x}}\mathbf{u}$, such that the real-space and hull representation coincide:

$$(2.4) \quad \nabla \mathbf{Y}_j^\omega(\mathbf{x}) = \mathbf{I} + (\nabla_{\mathbf{x}}\mathbf{u})(\mathbf{T}_{-\mathbf{x}}\omega).$$

2.2. Local disregistry in unmodulated and modulated configurations.

The energy landscape for interlayer interactions is tightly linked to the notion of disregistry, i.e. the relative shift between the layers. While this is a well-defined global quantity for commensurate lattices which are aligned, it can only be locally measured otherwise, and might change rapidly from one atom to its neighbor within one layer.

We are, however, particularly interested in this paper in the case where the lattices $\mathcal{R}_1, \dots, \mathcal{R}_p$ are close:

$$(2.5) \quad |\mathbf{I} - \mathbf{E}_i \mathbf{E}_j^{-1}| \ll 1, \text{ for all } 1 \leq i, j \leq p.$$

This condition leads to the emergence of moiré patterns with a characteristic length-scale much larger than the lattice constants.

In the reference (unrelaxed) state, the disregistry between two layers is well-defined. By definition, the configuration defined above for a lattice site of layer 1, for example, is the collection of its disregistries relative to the other layers, $(\gamma_j)_{2 \leq j \leq p}$. Note that the disregistry of the site with respect to the j -th layer is an element of Γ_j , and thus it is uniquely defined up to any element of \mathcal{R}_j .

This notion of disregistry can be extended smoothly to points of the layer plane which are not lattice sites using the following interpolation procedure. Given a point belonging to layer j in the configuration $(\gamma_1, \dots, \gamma_p) \in \Omega$, let us write $\gamma_j = \mathbf{E}_j \begin{bmatrix} s \\ t \end{bmatrix}$ with $0 \leq s, t < 1$. The nearest lattice sites in layer j are located at four points which form the four corners of a shifted unit cell of the lattice \mathcal{R}_j , as seen on Figure 3:

$$(2.6) \quad \mathbf{r}_{00} = \mathbf{E}_j \begin{bmatrix} s \\ t \end{bmatrix}, \quad \mathbf{r}_{10} = \mathbf{E}_j \begin{bmatrix} s-1 \\ t \end{bmatrix}, \quad \mathbf{r}_{01} = \mathbf{E}_j \begin{bmatrix} s \\ t-1 \end{bmatrix}, \quad \mathbf{r}_{11} = \mathbf{E}_j \begin{bmatrix} s-1 \\ t-1 \end{bmatrix}.$$

The respective disregistry of each of these four sites relative to the i -th layer is:

$$\gamma_i - \mathbf{r}_{00}, \quad \gamma_i - \mathbf{r}_{10} - \mathbf{E}_i \begin{bmatrix} 1 \\ 0 \end{bmatrix}, \quad \gamma_i - \mathbf{r}_{01} - \mathbf{E}_i \begin{bmatrix} 0 \\ 1 \end{bmatrix}, \quad \gamma_i - \mathbf{r}_{11} - \mathbf{E}_i \begin{bmatrix} 1 \\ 1 \end{bmatrix},$$

where an appropriate factor belonging to \mathcal{R}_i is introduced in each expression to keep the four disregistries clustered, assuming condition (2.5) is satisfied. Using bilinear interpolation in the variables s and t , we now compute the disregistry of layer i from the point of view of layer j in the configuration $(\gamma_1, \dots, \gamma_p)$:

$$\begin{aligned} \gamma_i - \mathbf{E}_j \begin{bmatrix} s \\ t \end{bmatrix} + (\mathbf{E}_j - \mathbf{E}_i) \left(s(1-t) \begin{bmatrix} 1 \\ 0 \end{bmatrix} + (1-s)t \begin{bmatrix} 0 \\ 1 \end{bmatrix} + st \begin{bmatrix} 1 \\ 1 \end{bmatrix} \right) &= \gamma_i - \mathbf{E}_i \begin{bmatrix} s \\ t \end{bmatrix} \\ &= \gamma_i - \mathbf{E}_i \mathbf{E}_j^{-1} \gamma_j. \end{aligned}$$

Note that this quantity is well-defined in Γ_i , periodic in both variables γ_i and γ_j . We can now give a meaning to the disregistry for any couple of layers in any configuration.

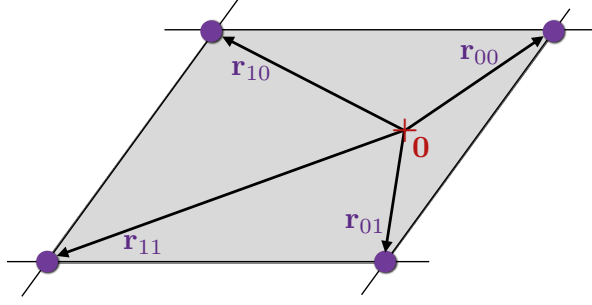


Fig. 3: Illustration of the shifted unit cell used for bilinear interpolation of disregistry.

DEFINITION 2.3. For any configuration $(\gamma_1, \dots, \gamma_p) \in \Omega$, we define the reference local disregistry $\mathbf{b}_{j \rightarrow i}$ of layer j with respect to layer i as the quantity

$$(2.7) \quad \mathbf{b}_{j \rightarrow i}(\gamma_1, \dots, \gamma_p) = \gamma_i - \mathbf{E}_i \mathbf{E}_j^{-1} \gamma_j \in \Gamma_i.$$

Note that the reference disregistry obeys the natural symmetry relation

$$\mathbf{E}_i^{-1} \mathbf{b}_{j \rightarrow i} = -\mathbf{E}_j^{-1} \mathbf{b}_{i \rightarrow j}.$$

In a deformed state, the local disregistry is shifted from its reference value due to the modulation fields. This can be modeled as follows.

DEFINITION 2.4. Given a set of modulation fields $(\mathbf{u}_j)_{1 \leq j \leq p}$, we define the modulated local disregistry $\mathbf{B}_{j \rightarrow i}$ of layer j with respect to layer i as the quantity

$$(2.8) \quad \mathbf{B}_{j \rightarrow i}(\omega) := \mathbf{b}_{j \rightarrow i}(\omega) + \mathbf{u}_i(\omega) - \mathbf{u}_j(\omega) \in \Gamma_i.$$

2.3. Atomistic kinematics. In the context of atomistic models of the elastic behavior of the structures, the dimension of the hull $\Omega = \Gamma_1 \times \dots \times \Gamma_p$ on which we define our modulation functions can be reduced. Indeed, only the displacement of atoms is well defined in such models, while arbitrary points in the layer planes have no prescribed position after deformation. This leads us to introduce the so-called *transversal of the hull*, denoted by X , which is formed as the set

$$(2.9) \quad X = \{(j, \omega) \mid 1 \leq j \leq p, \omega = (\gamma_1, \dots, \gamma_p) \in \Omega, \gamma_j = \mathbf{0}\}.$$

The idea is that elements of X represent a possible unique viewpoint from the position of a lattice site, rather than an arbitrary point in the layer plane as does Ω .

Following the formalism introduced in the previous section, an atomistic displacement is then a map $\mathbf{u} : X \rightarrow \mathbb{R}^2$. We will use the notation $\mathbf{u}_j(\omega) := \mathbf{u}(j, \omega)$ for the evaluation of functions defined on X , and we call $\mathbf{u}_j(\omega)$ the deformed position of an atom of layer j in the configuration ω .

REMARK 2.5. As in the continuum case, we assume here that all degrees of freedom are located at the Bravais lattice sites, and we do not deal with the multilattice case. This simplification can be viewed as an approximation where all atoms in the unit cell share the same displacement.

2.4. Local disregistry for atomistic deformations. In the case of atomistic deformations, it is not so easy to define the modulated local disregistry as in the continuum case (2.8). Indeed, the deformation of two different layers is not defined at the same point in general. A first idea to overcome this difficulty is to interpolate the displacements of the closest sites as earlier for the definition of the reference local disregistry.

Let $\omega = (\gamma_1, \dots, \gamma_p) \in \Omega$ be an arbitrary configuration. Consider a particular layer j and write $\gamma_j = E_j \begin{bmatrix} s \\ t \end{bmatrix}$ with $0 \leq s, t < 1$. The nearest lattice sites in layer j are located at the four points \mathbf{r}_{ab} with $a, b \in \{0, 1\}$ defined as in (2.6). Then, the bilinear interpolant of the atomic displacement of layer j at the origin is

$$(2.10) \quad \begin{aligned} \tilde{\mathbf{u}}_j(\omega) = & (1-s)(1-t) \mathbf{u}_j(\mathbf{T}_{-\mathbf{r}_{00}}\omega) + s(1-t) \mathbf{u}_j(\mathbf{T}_{-\mathbf{r}_{10}}\omega) \\ & + (1-s)t \mathbf{u}_j(\mathbf{T}_{-\mathbf{r}_{01}}\omega) + st \mathbf{u}_j(\mathbf{T}_{-\mathbf{r}_{11}}\omega). \end{aligned}$$

The deformation field $\tilde{\mathbf{u}}_j$ is a smooth interpolant which allows us to lift the atomistic displacement defined on the transversal X to a set of continuous displacement fields defined on Ω , for each of the layer planes.

REMARK 2.6. *Alternatives could be proposed for this spatial interpolant (2.10), for example using linear interpolation on any triangular mesh based on the lattice, or also higher-order schemes.*

A second idea is to avoid the construction of the interpolant (2.10) by instead evaluating the atomistic displacement at the (interpolated) local disregistry of layer j with respect to the other layers:

$$(2.11) \quad \hat{\mathbf{u}}_j(\omega) = \mathbf{u}_j(\Pi_j\omega),$$

where we have introduced the configuration interpolant $\Pi_j : \Omega \rightarrow \Omega$ defined by

$$(2.12) \quad \Pi_j\omega = (\mathbf{b}_{j \rightarrow 1}(\omega), \dots, \mathbf{b}_{j \rightarrow p}(\omega)) \quad \text{so that} \quad (j, \Pi_j\omega) \in X.$$

REMARK 2.7. *There does not seem to be any natural alternatives to the configuration interpolant (2.11).*

Any spatial interpolant such as (2.10) only relies on proximity in *physical* space. The accuracy of a method based on its use can be certified, in the sense that it can be framed in the context of well understood atomistic-to-continuum methods [27]. While much easier to use, the configuration interpolant (2.11) relies on proximity in *configuration* space, so its accuracy is not so readily analyzed. Within the context of the one-dimensional Frenkel-Kontorova model a full analysis is possible and indicates that the behavior in configuration space is smooth in the perturbative regime, but becomes fully discontinuous (Cantor-like) after the commensurate-incommensurate transition. The configuration-based interpolant essentially smoothes out this discontinuous behavior.

Let us highlight how the difference between the two proposed approaches is quantified by smoothness in configuration space with the following analysis. Since the local disregistry varies slowly, at the scale of the moiré pattern, both approaches are very close as long as the atomic displacement \mathbf{u} is smooth enough as a function of the configuration parameter. In particular, if \mathbf{u}_j is (locally) linear in ω then the two displacement interpolants (2.10) and (2.11) are in fact equal. This observation is the basis of the following estimate, which we prove in Appendix A

PROPOSITION 2.8.

$$(2.13) \quad \|\hat{\mathbf{u}}_j - \tilde{\mathbf{u}}_j\|_{L^q(\Omega)} \leq \left(\frac{|\Gamma_j|}{2q+1} \right)^{1/q} \theta^2 \|\nabla_\omega^2 \mathbf{u}_j\|_{L^q(X_j)}$$

where $X_j = \times_{i \neq j} \Gamma_i$ is the subset of the transversal corresponding to lattice sites of layer j , $\nabla_\omega^2 \mathbf{u}_j$ is understood as a 2-linear form for which the norm is defined as $\|\ell\| := \sup_{|\mathbf{h}_1|=|\mathbf{h}_2|=1} |\ell[\mathbf{h}_1, \mathbf{h}_2]|$ and

$$(2.14) \quad \theta = \sqrt{p} \sup_{1 \leq i, j \leq p} \|\mathbf{E}_i - \mathbf{E}_j\|, \quad \text{where } \|\cdot\| \text{ denotes the } \mathbb{R}^2\text{-operator norm.}$$

Based on these interpolants, we may finally define the local disregistry in the modulated atomic configuration:

DEFINITION 2.9. *Given an atomistic displacement \mathbf{u} , we define the modulated local disregistries $\tilde{\mathbf{B}}_{j \rightarrow i}$ and $\hat{\mathbf{B}}_{j \rightarrow i}$ of a site of layer j with respect to layer i :*

$$(2.15) \quad \Gamma_i \ni \tilde{\mathbf{B}}_{j \rightarrow i}(\omega) := \mathbf{b}_{j \rightarrow i}(\omega) + \tilde{\mathbf{u}}_i(\omega) - \tilde{\mathbf{u}}_j(\omega), \quad \text{for } (i, \omega) \in X,$$

and

$$(2.16) \quad \Gamma_i \ni \hat{\mathbf{B}}_{j \rightarrow i}(\omega) := \mathbf{b}_{j \rightarrow i}(\omega) + \hat{\mathbf{u}}_i(\omega) - \hat{\mathbf{u}}_j(\omega), \quad \text{for } (i, \omega) \in X.$$

3. Elastic models of relaxation. Let us now introduce elastic models of moiré pattern relaxation based on the previously introduced configuration-based parameterization of the deformation. We discuss a general atomistic energy model. Subsequently, we discuss a continuum model and how it is an effective approximation for the atomistic model.

3.1. The atomistic energy. We first formulate an atomistic model with empirical multi-body interactions. We admit deformations of the form (2.2):

$$\mathbf{Y}_j^\omega(\boldsymbol{\xi}) = \boldsymbol{\xi} + \mathbf{u}_j(\mathbf{T}_{-\boldsymbol{\xi}}\omega), \quad 1 \leq j \leq p, \quad \boldsymbol{\xi} \in \gamma_j + \mathcal{R}_j,$$

where $\mathbf{u} : X \rightarrow \mathbb{R}^2$ is an unknown displacement and $\omega = (\gamma_1, \dots, \gamma_p)$ a given configuration. We now propose a formal definition of the atomistic potential energy, which we make rigorous through the remainder of the section. Let $\mathcal{B}_j = \mathcal{R}_j \setminus \{\mathbf{0}\}$ denote intra-layer lattice directions or bonds. For discrete maps $\mathbf{v} : X \rightarrow \mathbb{R}^2$ we define the finite difference stencils:

$$(3.1) \quad D_j \mathbf{v}(j, \omega) := (\mathbf{v}_j(\mathbf{T}_{-\rho}\omega) - \mathbf{v}_j(\omega))_{\rho \in \mathcal{B}_j}, \quad \text{for } (j, \omega) \in X,$$

$$(3.2) \quad \Delta_{ij} \mathbf{v}(j, \omega) := (\mathbf{v}_i(\mathbf{T}_{-\rho}\omega) - \mathbf{v}_j(\omega))_{\rho \in \gamma_i + \mathcal{R}_i}, \quad \text{for } (j, \omega) \in X \text{ and } i \neq j.$$

Next, we assume that there exists a many-body site energy V_j for atoms in layer j such that, formally, the atomistic potential energy can be presented as a sum over normalized site-energies

$$(3.3) \quad \mathcal{E}^a(\mathbf{u}) := \sum_{j=1}^p \sum_{\boldsymbol{\xi} \in \gamma_j + \mathcal{R}_j} |\Gamma_j| \Phi_{j, \mathbf{T}_{-\boldsymbol{\xi}}\omega}(\mathbf{u}) \quad \text{where } \Phi_{j, \omega}(\mathbf{u}) := V_j [D_j \mathbf{u}, \{\Delta_{ij} \mathbf{u}\}_{i \neq j}](j, \omega).$$

This quantity is not well-defined for general displacement \mathbf{u} , and in fact the sum (3.3) does not exist in general for nonzero displacements \mathbf{u} which are continuous on the

configuration space X . However the corresponding atomistic potential energy by unit area is well-defined in the thermodynamic limit:

$$(3.4) \quad E^a(\mathbf{u}) := \lim_{r \rightarrow \infty} \sum_{j=1}^p \frac{|\Gamma_j|}{|B_r|} \sum_{\xi \in B_r \cap (\gamma_j + \mathcal{R}_j)} \Phi_{j, \tau_{-\xi} \omega}(\mathbf{u}).$$

Indeed, the Birkhoff property (1.5) allows us to express directly the large volume spatial average as a simple average over the configuration space:

$$(3.5) \quad E^a(\mathbf{u}) = \sum_{j=1}^p \int_{X_j} \Phi_{j, \omega}(\mathbf{u}),$$

where we recall that $X_j = \times_{i \neq j} \Gamma_i$ is the transversal of the configuration space corresponding to lattice sites of layer j . The definition (3.5) of an elastic energy for relaxed stackings is completely general and establishes the basis of an atomistic model for arbitrary incommensurate stackings which will be studied in forthcoming papers. As a first step, we focus in this paper on showing how a simple continuous model can be formulated under the moiré assumption (2.5).

3.2. Assumptions on the interaction potentials.

3.2.1. Separation of intra- and inter-layer contributions. The physical nature of the bonds between atoms of one layer is typically different, and of a much stronger nature, than the van der Waals interactions between adjacent layers. In particular, the bonding of atoms within an individual layer is mostly independent of the arrangement of the other layers. Furthermore, the most significant contribution of interactions between different layers is a misfit energy due to the local disregistry between adjacent layers.

To reflect these considerations, we propose the site energy for atoms of layer j :

$$(3.6) \quad \Phi_{j, \omega}(\mathbf{u}) = \Phi_{j, \omega}^{\text{intra}}(\mathbf{u}) + \eta \Phi_{j, \omega}^{\text{inter}}(\mathbf{u}),$$

where $0 < \eta \ll 1$ is a small positive parameter controlling the strength of the inter-layer van der Waals interactions. We make the form of each term $\Phi_{j, \omega}^{\text{intra}}$ and $\Phi_{j, \omega}^{\text{inter}}(\mathbf{u})$ explicit below. The equilibrium multilayer structure is obtained by minimizing the total energy (3.5) with respect to the displacement field \mathbf{u} . The competition between the intra-layer elastic (distortion) energy (3.7) and inter-layer misfit (disregistry) energy (3.17) thus drives the deviation from the perfect (unrelaxed) moiré.

3.2.2. Intra-layer elastic energy. The intra-layer contribution Φ^{intra} writes:

$$(3.7) \quad \Phi_{j, \omega}^{\text{intra}}(\mathbf{u}) := V_j^{\text{intra}}(D_j \mathbf{u}_j(\omega)).$$

Individual layers are simply two dimensional crystals, so the study of the corresponding internal elastic energy deriving from the potential V_j^{intra} (3.7) is classical. For the sake of completeness, we recall here some basic assumptions which ensure a proper definition of the intra-layer atomistic potential energy,

$$(3.8) \quad E_j^a(\mathbf{u}_j) := \int_{X_j} V_j^{\text{intra}}(D_j \mathbf{u}_j(\omega)).$$

Following [27], we define the intra-layer finite difference stencil space

$$(3.9) \quad \mathcal{D}_j := \{ \mathbf{g} = (g_\rho)_{\rho \in \mathcal{B}_j} \mid g_\rho \in \mathbb{R}^2, \|g\|_{\mathcal{D}_j} < \infty \},$$

equipped with the norm $\|\mathbf{g}\|_{\mathcal{D}_j} := \sup_{\rho \in \mathcal{B}_j} |g_\rho|/|\rho|$. Furthermore, to avoid difficulties associated with a possible lack of injectivity, we place an L^∞ -bound on the displacement gradient. This could be ensured by conditions on the weakness of inter-layer interactions, i.e., η small enough. In practice, we set a constant $0 < \kappa < 1$, $\mathcal{D}_{j,\kappa} := \{\mathbf{g} \in \mathcal{D}_j \mid \|\mathbf{g}\|_{\mathcal{D}_j} \leq \kappa\}$, and

$$(3.10) \quad \mathcal{K} = \{\mathbf{u} : X \rightarrow \mathbb{R}^2 \mid D_j \mathbf{u}(j, \omega) \in \mathcal{D}_{j,\kappa}, \forall (j, \omega) \in X\}.$$

Energy difference. We assume that $V_j^{\text{intra}}(\mathbf{0}) = 0$ for all $1 \leq j \leq p$. This means that E_j^a is the potential energy difference per unit area between the deformed state $\mathbf{Y}_j^\omega(\boldsymbol{\xi}) = \boldsymbol{\xi} + \mathbf{u}_j(\mathbf{T}_{-\boldsymbol{\xi}}\omega)$, $\boldsymbol{\xi} \in \gamma_j + \mathcal{R}_j$, and the reference state $\mathbf{Y}_j^{\text{ref}}(\boldsymbol{\xi}) = \boldsymbol{\xi}$, $\boldsymbol{\xi} \in \mathcal{R}_j$.

Symmetry. We assume that V_j^{intra} satisfies the inversion symmetry:

$$V_j^{\text{intra}}((-g_{-\rho})_{\rho \in \mathcal{B}_j}) = V_j^{\text{intra}}(\mathbf{g}), \quad \forall \mathbf{g} \in \mathcal{D}_j.$$

Smoothness. We assume that $V_j^{\text{intra}} \in C^k(\mathcal{D}_{j,\kappa})$, for some $k \geq 2$: the potential is smooth for injective deformations. Partial derivatives are denoted as

$$V_{j,\boldsymbol{\rho}}^{\text{intra}}(\mathbf{g}) := \frac{\partial^i V_j^{\text{intra}}(\mathbf{g})}{\partial g_{\rho_1} \dots \partial g_{\rho_i}} \quad \text{for } \mathbf{g} \in \mathcal{D}_{j,\kappa} \text{ and } \boldsymbol{\rho} \in (\mathcal{B}_j)^i,$$

and understood as multilinear forms acting on families of vectors $\mathbf{h} = (h_1, \dots, h_i)$, denoted as $V_{j,\boldsymbol{\rho}}^{\text{intra}}(\mathbf{g})[\mathbf{h}] = V_{j,\rho_1 \dots \rho_i}^{\text{intra}}[h_1, \dots, h_i]$, equipped with the norm

$$(3.11) \quad \|\ell\| := \sup_{\mathbf{h} \in (\mathbb{R}^2)^i, |h_1| = \dots = |h_i| = 1} \ell[\mathbf{h}].$$

Decay hypothesis. Analysis of the intralayer atomistic potential energies requires a sufficiently rapid decay in the interatomic interactions. In particular, E_j^a is well defined and k -times Fréchet differentiable on \mathcal{K} if the potentials V_j^{intra} satisfy the basic bounds [27] on the quantities

$$(3.12) \quad M^{(i)} := \max_{1 \leq j \leq p} \sum_{\boldsymbol{\rho} \in (\mathcal{B}_j)^i} m_j(\boldsymbol{\rho}) < \infty, \quad \text{for } 1 \leq i \leq k,$$

where

$$m_j(\boldsymbol{\rho}) := \prod_{l=1}^i |\rho_l| \sup_{\mathbf{g} \in \mathcal{D}_{j,\kappa}} \|V_{j,\boldsymbol{\rho}}^{\text{intra}}(\mathbf{g})\| \quad \text{for } \boldsymbol{\rho} \in (\mathcal{B}_j)^i, \quad 1 \leq i \leq k.$$

Stability. We assume finally that the lattices \mathcal{R}_j are stable, that is,

$$(3.13) \quad \nu := \min_{1 \leq j \leq p} \inf_{\substack{\mathbf{v} \in C(X, \mathbb{R}^2) \\ \|\nabla \mathbf{v}\|_{L^2} = 1}} \delta^2 E_j^a(0)[\mathbf{v}, \mathbf{v}] > 0.$$

Physically, (3.13) ensures that small distortions of the lattice \mathcal{R}_j will increase the potential energy for layer j in the stack.

Cauchy-Born approximate energy density. The Cauchy-Born elastic energy density function $W: \mathbb{R}^{2 \times 2} \rightarrow \mathbb{R} \cup \pm\infty$ is as usual defined by

$$(3.14) \quad W_j(\mathbf{F}) := V_j^{\text{intra}}(\mathbf{F} \cdot \mathcal{B}_j).$$

When elastic deformations are smooth, the Cauchy-Born model is a popular approximation to the atomistic model E_j^a . Indeed, for a smooth real-space displacement $\mathbf{U}_j : \mathbb{R}^2 \rightarrow \mathbb{R}^2$ of atoms in layer j , $V_j^{\text{intra}}(D_j \mathbf{U}_j(\boldsymbol{\xi})) \approx V_j^{\text{intra}}(\nabla \mathbf{U}_j(\boldsymbol{\xi}) \cdot \mathcal{B}_j) = W_j(\nabla \mathbf{U}_j(\boldsymbol{\xi}))$. Note that the spatial gradient of the atomistic deformation only makes sense after an appropriate interpolant is constructed [27].

3.2.3. Inter-layer misfit energy. The leading order contribution to the local misfit energy between two neighboring, *slightly misaligned* layers j and $j + 1$, where $1 \leq j < p$ corresponds to the stacking-fault energy per unit area [32] of an isolated bilayer structure formed of layers j and $j + 1$ and slightly rotated or stretched into periodic alignment, which we interpret as a misfit energy functional $\Phi_{j,j+1}^{\text{misfit}}(\omega)$.

In practice, such a misfit energy has been shown in the physics literature to be most accurately described as a generalized stacking-fault energy [20] which can be determined from accurate Density Functional Theory calculations [14, 24]. Note that out-of-plane displacements can be taken into account by extending the definition of the misfit energy to include a variable interlayer spacing (3D GSFE) [16].

REMARK 3.1. *Due to the high cost of accurate first-principles calculations including van der Waals bonding corrections, this energy density is typically computed in the approximation where both layers share the same lattice, $E_a = E_b$, or form a small supercell. Such functionals are directly available in the literature for a number of layer combinations such as G/G , $G/h\text{BN}$ or $h\text{BN}/h\text{BN}$ involving graphene (G) or hexagonal boron nitride ($h\text{BN}$) monolayers [36]. More recently, such a functional has been given for MoS_2 in [10]. Alternatively, direct summation techniques based on empirical potentials such as the Kolmogorov-Crespi G/G potentials [22] have been developed, and may allow to take into account additional local stress dependence of the stacking fault energy [35].*

Because the stacking-fault energy naturally depends only on the local reference disregistry of the layers of interest, we further introduce the site-energies $\Phi_{j\pm}^{\text{misfit}} : \Gamma_{j\pm 1} \mapsto \mathbb{R}$ localized on each layer, defined by:

$$(3.15) \quad \Phi_{j+}^{\text{misfit}}(\mathbf{b}_{j \rightarrow (j+1)}(\omega)) = \Phi_{(j+1)-}^{\text{misfit}}(\mathbf{b}_{(j+1) \rightarrow j}(\omega)) = \Phi_{j,j+1}^{\text{misfit}}(\omega).$$

Note that by definition 2.7 of the local reference disregistry $\mathbf{b}_{j \rightarrow (j+1)}$, these site energies satisfy the symmetry relation:

$$(3.16) \quad \Phi_{(j+1)-}^{\text{misfit}}(E_j \mathbf{s}) = \Phi_{j+}^{\text{misfit}}(-E_{j+1} \mathbf{s}), \quad \mathbf{s} \in E_j^{-1} \Gamma_j = E_{j+1}^{-1} \Gamma_{j+1} \equiv [-1/2, 1/2)^2.$$

When the layers are relaxed, we propose to write the inter-layer contribution Φ^{inter} as:

$$(3.17) \quad \Phi_{j,\omega}^{\text{inter}}(\mathbf{u}) := \begin{cases} \frac{1}{2} \Phi_{1+}^{\text{misfit}}(\mathbf{B}_{1 \rightarrow 2}(\omega)), & \text{if } j = 1, \\ \frac{1}{2} \Phi_{j+}^{\text{misfit}}(\mathbf{B}_{j \rightarrow j+1}(\omega)) + \frac{1}{2} \Phi_{j-}^{\text{misfit}}(\mathbf{B}_{j \rightarrow j-1}(\omega)), & \text{if } 1 < j < p, \\ \frac{1}{2} \Phi_{p-}^{\text{misfit}}(\mathbf{B}_{p \rightarrow p-1}(\omega)), & \text{if } j = p, \end{cases}$$

where we recall that $\mathbf{B}_{j \rightarrow i}$ is the modulated local disregistry of layer j with respect to layer i defined earlier (2.8).

3.3. Continuum approximation. We now build a continuum model *on the atomistic configuration space X* . Note that the dimensionality is thus reduced compared to the continuum description on the full hull Ω described in Section 2.1.

The first step is to formulate the spatial gradient associated with a given deformation field \mathbf{u} . Instead of a traditional spatial interpolant such as (2.10), let us compute using the configuration interpolant introduced earlier (2.11),

$$\nabla_{\mathbf{x}} \hat{\mathbf{u}}_j(\omega) = - \sum_{i \neq j} [\nabla_{\gamma_i} \mathbf{u}_j](\Pi_j \omega) - \sum_{i \neq j} [\nabla_{\gamma_i} \mathbf{u}_j](\Pi_j \omega) \cdot (-E_i E_j^{-1}).$$

Evaluating at a point $(j, \omega) \in X$, so that $\Pi_j \omega = \omega$, we obtain the spatial gradient of the atomistic displacement:

$$(3.18) \quad \widehat{\nabla}_{\mathbf{x}} \mathbf{u}_j := \sum_{i \neq j} \nabla_{\gamma_i} \mathbf{u}_j \cdot (\mathbf{E}_i \mathbf{E}_j^{-1} - \mathbf{I}).$$

Next, we define a continuous elastic energy density approximating E_j^a as well as an overall intra-layer energy density, using the Cauchy-Born approximation (3.14):

$$(3.19) \quad E_j^c(\mathbf{u}_j) := \int_{X_j} W_j(\widehat{\nabla}_{\mathbf{x}} \mathbf{u}_j), \quad E^{\text{CB}}(\mathbf{u}) := \sum_{j=1}^p E_j^c(\mathbf{u}_j),$$

as well as an inter-layer misfit energy density:

$$(3.20) \quad E^{\text{misfit}}(\mathbf{u}) = \frac{1}{2} \sum_{j=1}^{p-1} \int_{X_j} \Phi_{j+}^{\text{misfit}}(\widehat{\mathbf{B}}_{j \rightarrow j+1}(\omega)) + \frac{1}{2} \sum_{j=2}^p \int_{X_j} \Phi_{j-}^{\text{misfit}}(\widehat{\mathbf{B}}_{j \rightarrow j-1}(\omega)),$$

where we have used the interpolated modulated local disregistry $\widehat{\mathbf{B}}_{j \rightarrow j \pm 1}$ defined earlier (2.16):

$$\Gamma_{j \pm 1} \ni \widehat{\mathbf{B}}_{j \rightarrow j \pm 1} = \gamma_{j \pm 1} + \mathbf{u}_{j \pm 1}(\Pi_{j \pm 1} \omega) - \mathbf{u}_j(\omega), \quad \text{for } (j, \omega) \in X.$$

Finally, we formulate the Cauchy-Born elastostatics model for multilayers:

$$(3.21) \quad \mathbf{u}^c \in \arg \min \{ E^{\text{CB}}(\mathbf{u}) + \eta E^{\text{misfit}}(\mathbf{u}) \mid \mathbf{u} \in H^1 \cap W^{1, \infty}(X; \mathbb{R}^2) \},$$

and we understand (3.21) to be a *local* minimization problem [5] with respect to the $H^1 \cap W^{1, \infty}$ topology.

REMARK 3.2. *Here we do not include possible external uniform/periodic forces in our formulation, although our analysis extends this case in a straightforward manner.*

REMARK 3.3. *We also do not include out of plane bending in our presentation, though we note all the analysis could be extended to include bending. In this case, the intra-layer continuum model would become more complex to include curvature effects, and the modulated disregistry would need to include parallax effects due to out of plane bending as in [16].*

4. Analytical study and results: bilayer case. In this section, we present a first result on the existence of minimizers for the relaxation problem (3.21). We limit our current scope to the case of bilayers ($p = 2$). Note that there are additional difficulties linked with the degenerate ellipticity of the energy functional E^{CB} for $p \geq 3$, and we postpone to later studies their investigation.

4.1. The moiré cell for bilayers. Let us fix $p = 2$. In this case, the configuration space is simply $\Omega = \Gamma_1 \times \Gamma_2$ and the transversal for each layer is simply $X_1 = \Gamma_2$, $X_2 = \Gamma_1$. The analysis can be simplified by an appropriate change of variables: let us define the moiré lattice

$$\mathcal{R}_{\mathcal{M}} := (\mathbf{E}_2^{-1} - \mathbf{E}_1^{-1})^{-1} \mathbb{Z}^2,$$

and the associated periodic moiré cell:

$$(4.1) \quad \Gamma_{\mathcal{M}} := \mathbb{R}^2 / \mathcal{R}_{\mathcal{M}} \equiv (\mathbf{E}_2^{-1} - \mathbf{E}_1^{-1})^{-1} [-1/2, 1/2]^2.$$

We introduce next the linear mappings

$$(4.2) \quad \gamma_1 : \begin{cases} \Gamma_{\mathcal{M}} \rightarrow \Gamma_1, \\ \mathbf{x} \mapsto (\mathbf{E}_1 \mathbf{E}_2^{-1} - \mathbf{I})\mathbf{x}, \end{cases} \quad \gamma_2 : \begin{cases} \Gamma_{\mathcal{M}} \rightarrow \Gamma_2, \\ \mathbf{x} \mapsto (\mathbf{E}_2 \mathbf{E}_1^{-1} - \mathbf{I})\mathbf{x}. \end{cases}$$

One checks easily that γ_1 and γ_2 are isomorphisms that satisfy $\Pi_1(\gamma_1, 0) = (0, \gamma_2)$ and $\Pi_2(0, \gamma_2) = (\gamma_1, 0)$. Using these as change of variables, we introduce the new displacement unknowns defined on the new domain $\Gamma_{\mathcal{M}}$:

$$(4.3) \quad \mathbf{u}_{\mathcal{M},1}(\mathbf{x}) := \mathbf{u}_1(\gamma_2(\mathbf{x})), \quad \mathbf{u}_{\mathcal{M},2}(\mathbf{x}) := \mathbf{u}_2(\gamma_1(\mathbf{x})).$$

One of the advantages of working on the domain $\Gamma_{\mathcal{M}}$ is that the spatial gradient defined earlier (3.18) corresponds by the chain rule to the normal gradient:

$$(4.4) \quad \nabla \mathbf{u}_{\mathcal{M},1}(\mathbf{x}) = \widehat{\nabla}_{\mathbf{x}} \mathbf{u}_1(\gamma_2(\mathbf{x})), \quad \nabla \mathbf{u}_{\mathcal{M},2}(\mathbf{x}) = \widehat{\nabla}_{\mathbf{x}} \mathbf{u}_2(\gamma_1(\mathbf{x})).$$

Let us finally reformulate the minimization problem (3.21) on the new domain $\Gamma_{\mathcal{M}}$:

$$(4.5) \quad (\mathbf{u}_{\mathcal{M},1}^c, \mathbf{u}_{\mathcal{M},2}^c) \in \arg \min \left\{ E_{\mathcal{M}}^{\text{CB}}(\mathbf{u}_{\mathcal{M},1}, \mathbf{u}_{\mathcal{M},2}) + \eta E_{\mathcal{M}}^{\text{misfit}}(\mathbf{u}_{\mathcal{M},1}, \mathbf{u}_{\mathcal{M},2}) \right. \\ \left. \mid \mathbf{u}_{\mathcal{M},1}, \mathbf{u}_{\mathcal{M},2} \in H^1 \cap W^{1,\infty}(\Gamma_{\mathcal{M}}; \mathbb{R}^2) \right\}$$

where

$$(4.6a) \quad E_{\mathcal{M}}^{\text{CB}}(\mathbf{u}_{\mathcal{M},1}, \mathbf{u}_{\mathcal{M},2}) := \int_{\Gamma_{\mathcal{M}}} W_1(\nabla \mathbf{u}_{\mathcal{M},1}) + W_2(\nabla \mathbf{u}_{\mathcal{M},2}),$$

and

$$(4.6b) \quad E_{\mathcal{M}}^{\text{misfit}}(\mathbf{u}_1, \mathbf{u}_2) := \frac{1}{2} \int_{\Gamma_{\mathcal{M}}} \Phi_{1+}(\gamma_2(\mathbf{x}) + \mathbf{u}_{\mathcal{M},2}(\mathbf{x}) - \mathbf{u}_{\mathcal{M},1}(\mathbf{x})) \\ + \Phi_{2-}(\gamma_1(\mathbf{x}) + \mathbf{u}_{\mathcal{M},1}(\mathbf{x}) - \mathbf{u}_{\mathcal{M},2}(\mathbf{x})) \, d\mathbf{x}.$$

In the remainder of the section, we will drop the index \mathcal{M} for simplicity whenever it is possible to do so without confusion.

4.2. The space of admissible displacements. Now, it is easy to notice that the atomistic and continuum models are both formally translation invariant:

$$E^a(\mathbf{u} + \mathbf{x}) = E^a(\mathbf{u}), \quad E^{\text{CB}}(\mathbf{u} + \mathbf{x}) = E^{\text{CB}}(\mathbf{u}), \quad E^{\text{misfit}}(\mathbf{u} + \mathbf{x}) = E^{\text{misfit}}(\mathbf{u}), \quad \forall \mathbf{x} \in \mathbb{R}^2.$$

In fact, the translation of each layer by independent vectors $\mathbf{x}_1, \mathbf{x}_2$ corresponds formally to choosing a different initial configuration, and in principle does not modify the energy landscape. Due to the approximation introduced by the interpolation scheme (Section 2.3), the misfit energy (3.20) is not exactly invariant under such independent translations of the layers; nevertheless these considerations justify formally the following additional constraint on modulation functions:

$$(4.7) \quad \int_{\Gamma_{\mathcal{M}}} \mathbf{u}_j = \mathbf{0}, \quad \text{for } j = 1, 2.$$

This leads us to introduce Sobolev spaces of periodic, null-average modulation functions for $n \geq 1$: on an arbitrary domain Γ :

$$(4.8) \quad W_{\#}^{n,p}(\Gamma) := \left\{ \mathbf{u} \in W^{n,p}(\Gamma, \mathbb{R}^2 \times \mathbb{R}^2) \text{ such that } \int_{\Gamma} \mathbf{u}_1 = \int_{\Gamma} \mathbf{u}_2 = \mathbf{0} \right\}, \\ W_{\#}^{\infty}(\Gamma) := \left\{ \mathbf{v} \in C^{\infty}(\Gamma, \mathbb{R}^2 \times \mathbb{R}^2) \text{ such that } \int_{\Gamma} \mathbf{v}_1 = \int_{\Gamma} \mathbf{v}_2 = \mathbf{0} \right\}.$$

We typically omit the explicit dependency on Γ when it is possible to do so without confusion, e.g. in this section $\Gamma \equiv \Gamma_{\mathcal{M}}$. The Hilbert space $W_{\#}^{n,2}$ is equipped with the norm:

$$(4.9) \quad \|\mathbf{u}\|_{n,2} := \left(\sum_{k=0}^n \|\nabla^k \mathbf{u}\|_{L^2}^2 \right)^{1/2}, \quad \text{where } \|\cdot\|_{L^2} = \left(\int_{\Gamma} \|\cdot\|^2 d\mathbf{x} \right)^{1/2}.$$

Finally, to avoid interpenetration of matter we assume that displacement gradients satisfy a uniform bound, and we define

$$(4.10) \quad K := \left\{ \mathbf{u} \in W_{\#}^{1,\infty}(\Gamma_{\mathcal{M}}) \mid \|\nabla \mathbf{u}_1\|_{L^\infty} \leq \kappa, \|\nabla \mathbf{u}_2\|_{L^\infty} \leq \kappa \right\},$$

where κ is the same constant as in the definition of \mathcal{K} (3.10). The stability of the layers in the continuous framework can be expressed by the following result, adapted from [27], Proposition 5.1 and Lemma 5.2:

PROPOSITION 4.1. *Suppose the lattices $\mathcal{R}_1, \mathcal{R}_2$ are stable and let ν be defined by (3.13), then*

$$(4.11) \quad \delta^2 E_{\mathcal{M}}^{\text{CB}}(\mathbf{0})[\mathbf{v}, \mathbf{v}] \geq \nu \|\nabla \mathbf{v}\|_{L^2}^2, \quad \forall \mathbf{v} \in W_{\#}^{1,2}.$$

Furthermore, there exists $\kappa_1 > 0$ such that, for $\kappa < \kappa_1$,

$$(4.12) \quad \delta^2 E_{\mathcal{M}}^{\text{CB}}(\mathbf{u})[\mathbf{v}, \mathbf{v}] \geq \frac{1}{2} \nu \|\nabla \mathbf{v}\|_{L^2}^2, \quad \forall \mathbf{v} \in W_{\#}^{1,2}, \quad \forall \mathbf{u} \in K.$$

Proof. As a first step, we note that the interpolant $\hat{\mathbf{u}}_j$ defined above (2.11) allows us by straightforward calculations to write the following Birkhoff averaging formula. Fix $\mathbf{u}_{\mathcal{M},j} \in K$, $j \in \{1, 2\}$, and $f \in C(\{\mathbf{F} \in \mathbb{R}^{2 \times 2}, |\mathbf{F}| \leq \kappa\})$, then for any $\omega \in \Omega$:

$$\int_{\Gamma_{\mathcal{M}}} f(\nabla \mathbf{u}_{\mathcal{M},j}) = \int_{\Omega} f(\nabla_{\mathbf{x}} \hat{\mathbf{u}}_j) d\mathbb{P} = \lim_{R \rightarrow \infty} \frac{1}{|B_R|} \int_{B_R} f(\nabla_{\mathbf{x}} \hat{\mathbf{u}}_j(\mathbf{T}_{-\mathbf{x}} \omega)) d\mathbf{x}.$$

Now let us show that (4.11) holds. Fix $\mathbf{v}_{\mathcal{M},j} \in C^\infty(\Gamma_{\mathcal{M}}, \mathbb{R}^2)$ and $\omega \in \Omega$. Let $\bar{\mathbf{v}}_j \in C^\infty(\mathbb{R}^2, \mathbb{R}^2)$ defined by $\bar{\mathbf{v}}_j(\mathbf{x}) = \mathbf{v}_j(\mathbf{T}_{-\mathbf{x}} \omega)$, such that (see also [27], Proposition 3.2):

$$\begin{aligned} \delta^2 E_{\mathcal{M},j}^{\text{CB}}(\mathbf{0})[\mathbf{v}_{\mathcal{M},j}, \mathbf{v}_{\mathcal{M},j}] &= \int_{\Gamma_{\mathcal{M}}} \nabla^2 W_j(\mathbf{0}) [\nabla \mathbf{v}_{\mathcal{M},j}, \nabla \mathbf{v}_{\mathcal{M},j}] \\ &= \lim_{R \rightarrow \infty} \frac{1}{|B_R|} \int_{B_R} \nabla^2 W_j(\mathbf{0}) [\nabla \bar{\mathbf{v}}_j, \nabla \bar{\mathbf{v}}_j] d\mathbf{x}, \end{aligned}$$

where $E_{\mathcal{M},j}^{\text{CB}}(\mathbf{v}_{\mathcal{M},j}) := \int_{\Gamma_{\mathcal{M}}} W_j(\nabla \mathbf{v}_{\mathcal{M},j})$. For $R > 0$, let $\phi_R \in C^\infty(\mathbb{R}^2, \mathbb{R})$ be a smooth cutoff function such that $0 \leq \phi_R \leq 1$, $\phi_R(\mathbf{x}) = 0$ for $|\mathbf{x}| \geq R + 1$, $\phi_R(\mathbf{x}) = 1$ for $|\mathbf{x}| \leq R$ and $\nabla \phi_R$ is uniformly bounded independently of R . By Lemma 5.2 in [27],

$$\int_{\mathbb{R}^2} \nabla^2 W_j(\mathbf{0}) [\nabla(\phi_R \bar{\mathbf{v}}_j), \nabla(\phi_R \bar{\mathbf{v}}_j)] d\mathbf{x} \geq \nu \int_{\mathbb{R}^2} |\nabla(\phi_R \bar{\mathbf{v}}_j)| \geq \nu \|\nabla \bar{\mathbf{v}}_j\|_{L^2(B_R)}^2.$$

Moreover

$$\begin{aligned} \int_{B_{R+1} \setminus B_R} \nabla^2 W_j(\mathbf{0}) [\nabla(\phi_R \bar{\mathbf{v}}_j), \nabla(\phi_R \bar{\mathbf{v}}_j)] d\mathbf{x} &\leq \|\nabla^2 W_j(\mathbf{0})\| \int_{B_{R+1} \setminus B_R} |\nabla(\phi_R \bar{\mathbf{v}}_j)|^2 \\ &\leq C(R+1) \|\nabla \bar{\mathbf{v}}_j\|_{L^2(B_{R+1} \setminus B_R)}^2, \end{aligned}$$

where $C > 0$ is a constant independent of R . We deduce in the thermodynamic limit:

$$\lim_{R \rightarrow \infty} \frac{1}{|B_R|} \int_{B_R} \nabla^2 W_j(\mathbf{0}) [\nabla \bar{\mathbf{v}}_j, \nabla \bar{\mathbf{v}}_j] d\mathbf{x} \geq \lim_{R \rightarrow \infty} \frac{\nu}{|B_R|} \|\nabla \bar{\mathbf{v}}_j\|_{L^2(B_R)}^2.$$

By the Birkhoff property above, this yields the configuration space estimate:

$$\delta^2 E_j^{\text{CB}}(\mathbf{0})[\mathbf{v}_{\mathcal{M},j}, \mathbf{v}_{\mathcal{M},j}] \geq \nu \|\nabla \mathbf{v}_{\mathcal{M},j}\|_{L^2}^2.$$

Then (4.11) follows by density of $W_{\#}^{\infty}$ in $W_{\#}^{1,2}$. The proof of (4.12) is analogous, using Proposition 5.1 in [27]. \square

Using the same idea, we can also prove the Lipschitz bounds on the variations of the intralayer energies as a consequence of Prop. 3.2 in [27]:

PROPOSITION 4.2. *Suppose the atomic potentials satisfy the decay bounds $M^{(k)} < \infty$ for $1 \leq k \leq 5$ where $M^{(k)}$ is defined by (3.12). Then for $k \leq 5$, $\sum_{i=1}^k \frac{1}{p_i} = 1$, we have*

$$(4.13) \quad \delta^k E_{\mathcal{M}}^{\text{CB}}(\mathbf{u})[\mathbf{v}_1, \dots, \mathbf{v}_k] \leq M^{(k)} \prod_{i=1}^k \|\nabla \mathbf{v}_i\|_{L^{p_i}}.$$

4.3. Existence of local energy minimizers. Our goal in this section is to prove the following existence theorem for the energy minimizer in the bilayer case:

THEOREM 4.3. *Suppose the lattices $\mathcal{R}_1, \mathcal{R}_2$ are stable in the sense of (3.13), then for η small enough there exists a solution $\mathbf{u}^c \in W_{\#}^{3,2}$ of the Euler-Lagrange equation,*

$$(4.14) \quad \delta E_{\mathcal{M}}^{\text{CB}}(\mathbf{u}^c)[\mathbf{v}] + \eta \delta E_{\mathcal{M}}^{\text{misfit}}(\mathbf{u}^c)[\mathbf{v}] = 0, \quad \forall \mathbf{v} \in W_{\#}^{3,2},$$

or equivalently is a solution of the two coupled partial differential equations on $\Gamma_{\mathcal{M}}$:

$$(4.15) \quad \begin{cases} -\mathbf{div}(\nabla W_1(\mathbf{u}_1)) = \eta \mathbf{f}(\mathbf{x}, \mathbf{u}_1 - \mathbf{u}_2), \\ -\mathbf{div}(\nabla W_2(\mathbf{u}_2)) = -\eta \mathbf{f}(\mathbf{x}, \mathbf{u}_1 - \mathbf{u}_2), \end{cases}$$

where $\mathbf{f}(\mathbf{x}, \mathbf{v}) := \frac{1}{2}(\nabla \Phi_{1+})[\gamma_2(\mathbf{x}) - \mathbf{v}] - \frac{1}{2}(\nabla \Phi_{2-})[\gamma_1(\mathbf{x}) + \mathbf{v}].$

Furthermore this solution is stable in the sense that there exists $c_0 > 0$ such that:

$$(4.16) \quad \delta^2 E_{\mathcal{M}}^{\text{CB}}(\mathbf{u}^c)[\mathbf{v}, \mathbf{v}] + \eta \delta^2 E_{\mathcal{M}}^{\text{misfit}}(\mathbf{u}^c)[\mathbf{v}, \mathbf{v}] \geq c_0 \|\mathbf{v}\|_{1,2}^2, \quad \forall \mathbf{v} \in W_{\#}^{1,2}.$$

REMARK 4.4. *The multi-well nature of the nonlinear forcing term in the right-hand side of the Euler-Lagrange equation (4.15) is reminiscent of the Ginzburg-Landau equation.*

REMARK 4.5. *The existence of global energy minimizers for arbitrary values of η can also be shown by standard methods exploiting the convexity properties of linear or nonlinear elastic functionals such as E^{CB} with respect to the gradient $\nabla_{\mathbf{x}} \mathbf{u}$ in the space of null-average displacements $W_{\#}^{1,p}$. The proofs of Theorem 9.5-2 in [13] in the linear case, or Theorem 8.31 in [15] for the non-linear case, apply almost verbatim with slight modifications to account for the periodic boundary conditions.*

Proof. Our proof relies on an application of the implicit functional theorem, for example Theorem 7.13-1 in [13] using the spaces $\mathcal{X} := \mathbb{R}$, $\mathcal{Y} := W_{\#}^{3,2}$ and $\mathcal{Z} := W_{\#}^{1,2}$ and a neighborhood of the origin $\mathcal{O} \subset \mathcal{X} \times \mathcal{Y}$ of the form:

$$\mathcal{O} := \{(\eta, \mathbf{u}) \in \mathbb{R} \times W_{\#}^{3,2} \mid |\eta| < \eta_0, \quad \|\mathbf{u}\|_{3,2} \leq \delta\},$$

where δ is chosen to be small enough that $\mathcal{O} \subset (-\eta_0, \eta_0) \times K$ thanks to the Sobolev embedding $W_{\#}^{3,2} \subset W_{\#}^{1,\infty}$. Define the mapping $\mathcal{F} : \mathcal{O} \rightarrow W_{\#}^{1,2}$ defined by

$$\mathcal{F}(\eta, \mathbf{u}) := \delta E_{\mathcal{M}}^{\text{CB}}(\mathbf{u}) + \eta \delta E_{\mathcal{M}}^{\text{misfit}}(\mathbf{u}).$$

We compute explicitly from (4.6), with \mathbf{f} defined as in (4.15):

$$(4.17) \quad \delta E_{\mathcal{M}}^{\text{CB}}(\mathbf{u}) = \begin{bmatrix} -\mathbf{div}(\nabla W_1(\nabla \mathbf{u}_1)) \\ -\mathbf{div}(\nabla W_2(\nabla \mathbf{u}_2)) \end{bmatrix}, \quad \delta E_{\mathcal{M}}^{\text{misfit}}(\mathbf{u}) = \begin{bmatrix} -\mathbf{f}(\mathbf{x}, \mathbf{u}_1 - \mathbf{u}_2) \\ \mathbf{f}(\mathbf{x}, \mathbf{u}_1 - \mathbf{u}_2) \end{bmatrix}.$$

The mapping \mathcal{F} satisfies $\mathcal{F}(0, \mathbf{0}) = \mathbf{0}$. Furthermore, using the Sobolev inequalities $\|\mathbf{u}\|_{1,\infty} \lesssim \|\mathbf{u}\|_{2,4} \lesssim \|\mathbf{u}\|_{3,2}$ and estimate (4.13), a lengthy but straightforward computation for arbitrary $\mathbf{u}, \mathbf{u}', \mathbf{v} \in W_{\#}^{3,2}$ leads to:

$$\begin{aligned} & \left\| \delta^2 E_{\mathcal{M}}^{\text{CB}}(\mathbf{u})[\mathbf{v}, \cdot] - \delta^2 E_{\mathcal{M}}^{\text{CB}}(\mathbf{u}')[\mathbf{v}, \cdot] \right\|_{1,2} \\ &= \left\| \begin{bmatrix} -\mathbf{div}(\nabla^2 W_1(\nabla \mathbf{u}_1) : \nabla \mathbf{v}_1 - \nabla^2 W_1(\nabla \mathbf{u}'_1) : \nabla \mathbf{v}_1) \\ -\mathbf{div}(\nabla^2 W_2(\nabla \mathbf{u}_2) : \nabla \mathbf{v}_2 - \nabla^2 W_2(\nabla \mathbf{u}'_2) : \nabla \mathbf{v}_2) \end{bmatrix} \right\|_{1,2} \\ &\leq C \sum_{k=3}^5 M^{(k)} \|\mathbf{u} - \mathbf{u}'\|_{3,2} \|\mathbf{v}\|_{3,2}, \end{aligned}$$

where C is a generic constant, independent of \mathcal{R}_1 and \mathcal{R}_2 . Similarly, we compute

$$\begin{aligned} & \left\| \delta^2 E_{\mathcal{M}}^{\text{misfit}}(\mathbf{u})[\mathbf{v}, \cdot] - \delta^2 E_{\mathcal{M}}^{\text{misfit}}(\mathbf{u}')[\mathbf{v}, \cdot] \right\|_{1,2} \\ &\leq \frac{1}{2} \sum_{j=1}^2 \left\| \begin{bmatrix} -(\nabla_{\mathbf{v}} \mathbf{f}_j(\mathbf{x}, \mathbf{u}_1 - \mathbf{u}_2) - \nabla_{\mathbf{v}} \mathbf{f}_j(\mathbf{x}, \mathbf{u}'_1 - \mathbf{u}'_2)) \cdot (\mathbf{v}_1 - \mathbf{v}_2) \\ (\nabla_{\mathbf{v}} \mathbf{f}_j(\mathbf{x}, \mathbf{u}_1 - \mathbf{u}_2) - \nabla_{\mathbf{v}} \mathbf{f}_j(\mathbf{x}, \mathbf{u}'_1 - \mathbf{u}'_2)) \cdot (\mathbf{v}_1 - \mathbf{v}_2) \end{bmatrix} \right\|_{1,2} \\ &\leq C \|\mathbf{u} - \mathbf{u}'\|_{W^{1,\infty}} \|\mathbf{v}\|_{W^{1,2}} \leq C' \|\mathbf{u} - \mathbf{u}'\|_{3,2} \|\mathbf{v}\|_{3,2}, \end{aligned}$$

with $C' = c \max_{j=1,2} (\kappa \|\nabla^4 \Phi_{j\pm}\|_{\infty} + \|\mathbf{E}_2 - \mathbf{E}_1\| \|\mathbf{E}_j^{-1}\| \|\nabla^4 \Phi_{j\pm}\|_{\infty} + \|\nabla^3 \Phi_{j\pm}\|_{L^{\infty}(K)})$ and c a generic constant. This shows that \mathcal{F} is continuously differentiable with respect to \mathbf{u} on Ξ :

$$\begin{aligned} \left\| \frac{\partial \mathcal{F}}{\partial \mathbf{u}}(\eta, \mathbf{u}) - \frac{\partial \mathcal{F}}{\partial \mathbf{u}}(\eta', \mathbf{u}') \right\|_{L(W_{\#}^{3,2}, W_{\#}^{1,2})} &\leq \sup_{\|\mathbf{v}\|_{3,2}=1} \left(\left\| \delta^2 E_{\mathcal{M}}^{\text{CB}}(\mathbf{u})[\mathbf{v}, \cdot] - \delta^2 E_{\mathcal{M}}^{\text{CB}}(\mathbf{u}')[\mathbf{v}, \cdot] \right\|_{1,2} \right. \\ &\quad \left. + \left\| \eta \delta^2 E_{\mathcal{M}}^{\text{misfit}}(\mathbf{u})[\mathbf{v}, \cdot] - \eta' \delta^2 E_{\mathcal{M}}^{\text{misfit}}(\mathbf{u}')[\mathbf{v}, \cdot] \right\|_{1,2} \right) \\ &\leq C (|\eta - \eta'| + \|\mathbf{u} - \mathbf{u}'\|_{3,2}). \end{aligned}$$

Finally, we observe that

$$\frac{\partial \mathcal{F}}{\partial \mathbf{u}}(0, \mathbf{0})[\mathbf{v}] = \delta^2 E_{\mathcal{M}}^{\text{CB}}(\mathbf{0})[\mathbf{v}, \cdot].$$

The second variation of the energy $\delta^2 E_{\mathcal{M}}^{\text{CB}}(\mathbf{0})$ is a continuous, coercive bilinear form on $W_{\#}^{1,2}$ thanks to Propositions 4.1, 4.2 and the Poincaré-Wirtinger inequality, and thus by the Lax-Milgram lemma for any $\mathbf{g} \in W_{\#}^{-1,2}$ there exists a unique solution \mathbf{u} to the problem:

$$\delta^2 E_{\mathcal{M}}^{\text{CB}}(\mathbf{0})[\mathbf{u}, \mathbf{v}] = (\mathbf{g}, \mathbf{v})_{L^2}, \quad \forall \mathbf{v} \in W_{\#}^{1,2}.$$

If in addition \mathbf{g} belongs to $W_{\#}^{1,2}$, then elliptic regularity (see [18], section 6.3.1) ensures that \mathbf{u} belongs to $W_{\#}^{3,2}$. This shows that $\delta^2 E_{\mathcal{M}}^{\text{CB}}(\mathbf{0})$ is a bijection from $W_{\#}^{3,2}$ to $W_{\#}^{1,2}$. Then, by the implicit function theorem there exists $\eta_0 > 0$ and $\delta > 0$ such that for $0 \leq \eta < \eta_0$, there exists a unique solution $\mathbf{u}^c(\eta)$ to the Euler-Lagrange equation, $\mathcal{F}(\eta, \mathbf{u}^c) = \mathbf{0}$, such that $\|\mathbf{u}^c\|_{3,2} < \delta$.

It remains to show that this solution is stable. As previously, we compute

$$\delta^2 E_{\mathcal{M}}^{\text{misfit}}(\mathbf{u}^c)[\mathbf{v}, \mathbf{v}] = \frac{1}{2} \sum_{j=1}^2 \int_{\Gamma_{\mathcal{M}}} (\mathbf{v}_1 - \mathbf{v}_2)^T \nabla_{\mathbf{v}} \mathbf{f}_j(\mathbf{x}, \mathbf{u}_1^c - \mathbf{u}_2^c) (\mathbf{v}_1 - \mathbf{v}_2) \geq -C \|\mathbf{v}\|_{L^2}^2,$$

where $C > 0$ is another generic constant. Proposition 4.1 then ensures that

$$(4.18) \quad \delta^2 E_{\mathcal{M}}^{\text{CB}}(\mathbf{u}^c)[\mathbf{v}, \mathbf{v}] + \eta \delta^2 E_{\mathcal{M}}^{\text{misfit}}(\mathbf{u}^c)[\mathbf{v}, \mathbf{v}] \geq \frac{\nu}{2} \|\nabla \mathbf{v}\|_{L^2}^2 - C\eta \|\mathbf{v}\|_{L^2}^2.$$

Then $\mathbf{u}^c(\eta)$ is a stable solution in the sense that (4.16) holds for $\eta < \min(\eta_0, \nu C_P^2/2C)$, where C_P is the constant in the Poincaré-Wirtinger estimate,

$$(4.19) \quad \|v - \langle v \rangle\|_{L^2(\Gamma_M)} \leq C_P \|\nabla v\|_{L^2(\Gamma_M)} \quad \text{where } \langle v \rangle = \int_{\Gamma_M} v d\mathbf{x}. \quad \square$$

4.4. Asymptotic analysis. Equations (4.18) and (4.19) together give a hint as to the regime where Theorem 4.3 ceases to apply: when $\|\mathbf{E}_1 - \mathbf{E}_2\| \rightarrow 0$, the size of the moiré cell grows to infinity. Then, the constant C_P in the Poincaré-Wirtinger estimate grows roughly as its diameter $\|(\mathbf{E}_1 - \mathbf{E}_2)^{-1}\|$. The physically relevant η value may become too large for Theorem 4.3 to apply. One possibility is for example that for large-scale moiré patterns, a bifurcation occurs where two or more stable solution branches exist [16].

To simplify the analysis, we will assume that both layers are made of the same material, and the stresses inside each layer are modeled by isotropic linear elasticity, i.e., the intralayer energy density functionals are the same $W := W_1 = W_2$ which takes the form

$$(4.20) \quad W(\mathbf{u}) = \frac{\lambda}{2} \text{div}(\mathbf{u})^2 + \mu \varepsilon(\mathbf{u}) : \varepsilon(\mathbf{u}) \quad \text{where } \varepsilon(\mathbf{u}) = \frac{1}{2}(\nabla \mathbf{u} + \nabla \mathbf{u}^T),$$

where $\lambda \geq 0$ and $\mu > 0$ are the Lamé parameters of the material. In addition, the lattices basis of both layers are identical, and thus share the same lattice basis \mathbf{E} simply twisted by a relative angle $\theta > 0$:

$$(4.21) \quad \mathbf{E}_1 = \mathbf{R}_{-\theta/2} \mathbf{E}, \quad \mathbf{E}_2 = \mathbf{R}_{\theta/2} \mathbf{E}, \quad \text{where } \mathbf{R}_{\theta} = \begin{bmatrix} \cos(\theta) & -\sin(\theta) \\ \sin(\theta) & \cos(\theta) \end{bmatrix}.$$

A direct computation then shows that for varying θ the moiré cell (4.1) is simply a rescaled copy of a new reference cell Γ_0 :

$$(4.22) \quad \Gamma_{\mathcal{M}}(\theta) = \frac{1}{2 \sin(\theta/2)} \Gamma_0, \quad \text{where } \begin{cases} \mathcal{R}_0 := \mathbf{E}_0 \mathbb{Z}^2, \\ \Gamma_0 := \mathbb{R}^2 / \mathcal{R}_0, \end{cases} \quad \text{with } \mathbf{E}_0 := \mathbf{R}_{-\pi/2} \mathbf{E}.$$

We rescale (4.2) to define consistent disregistry mappings on the reference cell Γ_0 :

$$(4.23) \quad \gamma_{1,\theta} : \begin{cases} \Gamma_0 \rightarrow \Gamma_1, \\ \mathbf{x} \mapsto -\mathbf{R}_{-\frac{\pi+\theta}{2}} \mathbf{x}, \end{cases} \quad \gamma_{2,\theta} : \begin{cases} \Gamma_0 \rightarrow \Gamma_2, \\ \mathbf{x} \mapsto \mathbf{R}_{\frac{\theta-\pi}{2}} \mathbf{x}. \end{cases}$$

Also, thanks to the symmetry relation (3.16) the generalized stacking fault energy can be transposed as a single functional:

$$(4.24) \quad \Phi_0(\mathbf{x}) := \Phi_{1+}(\gamma_{2,\theta}(\mathbf{x})) = \Phi_{2-}(\gamma_{1,\theta}(\mathbf{x})).$$

The Euler-Lagrange equation (4.15) for extremal points of the energy functional for any angle $0 < \theta < \pi$ can be recast as a problem on the reference cell Γ_0 :

$$(4.25) \quad \begin{cases} -\mathbf{div}(\lambda \mathbf{div}(\mathbf{u}_1)\mathbf{I} + 2\mu\varepsilon(\mathbf{u}_1)) = \frac{\eta}{4\sin^2(\theta/2)} \mathbf{F}_\theta(\mathbf{x}, \mathbf{u}_1 - \mathbf{u}_2), \\ -\mathbf{div}(\lambda \mathbf{div}(\mathbf{u}_2)\mathbf{I} + 2\mu\varepsilon(\mathbf{u}_2)) = \frac{-\eta}{4\sin^2(\theta/2)} \mathbf{F}_\theta(\mathbf{x}, \mathbf{u}_1 - \mathbf{u}_2), \end{cases}$$

where

$$(4.26) \quad \mathbf{F}_\theta(\mathbf{x}, \mathbf{v}) := \frac{1}{2} \nabla \Phi_0(\mathbf{x} - \mathbf{R}_{\frac{\pi-\theta}{2}} \mathbf{v}) \cdot \mathbf{R}_{\frac{\pi-\theta}{2}} + \frac{1}{2} \nabla \Phi_0(\mathbf{x} + \mathbf{R}_{\frac{\pi-\theta}{2}} \mathbf{v}) \cdot \mathbf{R}_{\frac{\pi+\theta}{2}}$$

It can be easily be shown that any solution of the system (4.25) satisfies $\mathbf{u}_1 = -\mathbf{u}_2$. Then the model (4.25) reduces simply to the single semilinear equation:

$$(4.27) \quad -\mathbf{div}(\lambda \mathbf{div}(\mathbf{u})\mathbf{I} + 2\mu\varepsilon(\mathbf{u})) = \frac{\eta}{4\sin^2(\theta/2)} \mathbf{F}_\theta(\mathbf{x}, 2\mathbf{u}), \quad \text{where } \mathbf{u} := \mathbf{u}_1 = -\mathbf{u}_2.$$

REMARK 4.6. *At small angles, a Taylor expansion of expression (4.26) indicates that F_θ depends only very weakly on θ :*

$$|F_\theta(\mathbf{x}, \mathbf{v}) - F_0(\mathbf{x}, \mathbf{v})| = \mathcal{O}(\theta^2 |\mathbf{v}|).$$

Therefore the main parameters governing the relaxation are the profile of the GSFE functional, mainly the location of the minima, saddle points and maxima which all depends mostly on the symmetries of the material, and the ratio of the GSFE amplitude to the square of the twist angle.

This explicit rescaling enables us to study explicitly the interplay between twist angle and strength of the interlayer coupling:

THEOREM 4.7. *Assume the functional Φ_0 is twice continuously differentiable.*

(a) *For any values of $\eta \geq 0$ and $\theta \neq n\pi$ for integer n there exists solutions to the Euler-Lagrange equation (4.27) in $W_{\#}^{1,2}(\Gamma_0)$, which satisfy*

$$(4.28) \quad \|\mathbf{u}^c\|_{1,2} \leq \frac{\|\nabla \Phi_0\|_{\infty}}{\mu C_{\mathbf{E}}^1} \frac{\eta}{4\sin^2(\theta/2)},$$

where $C_{\mathbf{E}}^1$ is a fully identifiable constant depending on the lattice basis \mathbf{E} only.

(b) *The solution is unique if*

$$(4.29) \quad \frac{\eta}{\theta^2} < \frac{\mu C_{\mathbf{E}}^0}{2\|\nabla^2 \Phi_0\|_{\infty}},$$

where $C_{\mathbf{E}}^0 > 2C_{\mathbf{E}}^1$ is another fully identifiable constant depending on the lattice basis \mathbf{E} only.

(c) If in addition Φ_0 is smooth, any solution is also smooth and its derivatives for any $k = 2, 3, \dots$ satisfy the bounds

$$(4.30) \quad \|\nabla^k \mathbf{u}^c\|_{L^2} \leq C_k \left| \frac{\sqrt{\eta}}{2 \sin(\theta/2)} \right|^k,$$

where the constant C_k depends only on E , μ and $\|\Phi_0\|_{C^{k+1}(\Gamma_0)}$.

Proof. Given any $\mathbf{g} \in L^2(\Gamma_0; \mathbb{R}^2)$, consider the problem: find \mathbf{u} such that

$$-\mathbf{div}(\lambda \mathbf{div}(\mathbf{u})\mathbf{I} + 2\mu\varepsilon(\mathbf{u})) = \mathbf{g}.$$

The corresponding variational formulation writes:

$$(4.31) \quad \int_{\Gamma_0} \lambda \mathbf{div}(\mathbf{u})\mathbf{div}(\mathbf{v}) + 2\mu\varepsilon(\mathbf{u}) : \varepsilon(\mathbf{v}) = \int_{\Gamma_0} \mathbf{g} \cdot \mathbf{v}, \quad \forall \mathbf{v} \in W^{1,2}(\Gamma_0, \mathbb{R}^2).$$

To establish the coercivity of the bilinear form on the left-hand side of (4.31), we decompose periodic, zero-average functions over Γ_0 as the Fourier series:

$$\mathbf{v}(\mathbf{x}) = \sum_{\mathbf{k} \in \mathcal{R}_0^* \setminus \{\mathbf{0}\}} \mathbf{v}_{\mathbf{k}} e^{2i\pi \mathbf{k} \cdot \mathbf{x}}, \quad \text{such that } \|\mathbf{v}\|_{1,2}^2 = \sum_{\mathbf{k} \in \mathcal{R}_0^*} (1 + |2\pi \mathbf{k}|^2) |\mathbf{v}_{\mathbf{k}}|^2.$$

Now we estimate:

$$\begin{aligned} \int_{\Gamma_0} \lambda \mathbf{div}(\mathbf{v})^2 + 2\mu\varepsilon(\mathbf{v}) : \varepsilon(\mathbf{v}) &\geq 2\mu \int_{\Gamma_0} \varepsilon(\mathbf{v}) : \varepsilon(\mathbf{v}) \\ &\geq 2\mu \sum_{\mathbf{k} \in \mathcal{R}_0^* \setminus \{\mathbf{0}\}} (2\pi)^2 \left| \frac{\mathbf{k} \otimes \mathbf{v}_{\mathbf{k}} + \mathbf{v}_{\mathbf{k}} \otimes \mathbf{k}}{2} \right|^2 \\ &\geq \mu \sum_{\mathbf{k} \in \mathcal{R}_0^* \setminus \{\mathbf{0}\}} |2\pi \mathbf{k}|^2 |\mathbf{v}_{\mathbf{k}}|^2. \end{aligned}$$

This implies the coercivity estimates:

$$(4.32) \quad \begin{aligned} \int_{\Gamma_0} \lambda \mathbf{div}(\mathbf{v})^2 + 2\mu\varepsilon(\mathbf{v}) : \varepsilon(\mathbf{v}) &\geq \mu \|\nabla \mathbf{v}\|_{L^2}^2, \\ \int_{\Gamma_0} \lambda \mathbf{div}(\mathbf{v})^2 + 2\mu\varepsilon(\mathbf{v}) : \varepsilon(\mathbf{v}) &\geq \mu C_E^0 \|\mathbf{v}\|_{L^2}^2, \\ \int_{\Gamma_0} \lambda \mathbf{div}(\mathbf{v})^2 + 2\mu\varepsilon(\mathbf{v}) : \varepsilon(\mathbf{v}) &\geq \mu C_E^1 \|\mathbf{v}\|_{1,2}^2, \end{aligned}$$

where $C_E^0 = \min\{|2\pi \mathbf{k}|^2 \mid \mathbf{k} \in \mathcal{R}_0^* \setminus \{\mathbf{0}\}\}$ and $C_E^1 = \frac{C_E^0}{1 + C_E^0}$. The Lax-Milgram lemma then ensures that there exists unique solutions $\mathcal{G}(\mathbf{g}) := \mathbf{u} \in W_{\#}^{1,2}$ to problem (4.31), such that \mathcal{G} is a continuous linear mapping $L^2 \rightarrow W_{\#}^{1,2}$ satisfying the bounds

$$\|\mathcal{G}(\mathbf{g})\|_{L^2} \leq \frac{1}{\mu C_E^0} \|\mathbf{g}\|_{L^2}, \quad \|\mathcal{G}(\mathbf{g})\|_{W_{\#}^{1,2}} \leq \frac{1}{\mu C_E^1} \|\mathbf{g}\|_{L^2}.$$

We also introduce the mapping $\mathcal{F} : L_{\#}^2 \rightarrow L^2$ with $\mathcal{F}(\mathbf{u}) = \frac{\eta}{4 \sin^2(\theta/2)} \mathbf{F}_{\theta}(\cdot, 2\mathbf{u}(\cdot))$, which is bounded: $\|\mathcal{F}(\mathbf{u})\|_{L^2} \leq \frac{\eta}{4 \sin^2(\theta/2)} \|\nabla \Phi_0\|_{\infty}$, as well as Lipschitz continuous:

$$\|\mathcal{F}(\mathbf{u}) - \mathcal{F}(\mathbf{u}')\|_{L^2} \leq \frac{2\eta}{4 \sin^2(\theta/2)} \|\nabla^2 \Phi_0\|_{\infty} \|\mathbf{u} - \mathbf{u}'\|_{L_{\#}^2}.$$

Now, we note that the mapping $\mathcal{H} = \mathcal{G} \circ \mathcal{F} : L_{\#}^2 \rightarrow W_{\#}^{1,2}$ is bounded,

$$(4.33) \quad \|\mathcal{H}(\mathbf{u})\|_{L^2} \leq \frac{\eta}{4 \sin^2(\theta/2)} \frac{\|\nabla \Phi_0\|_{\infty}}{\mu C_{\mathbb{E}}^0}, \quad \|\mathcal{H}(\mathbf{u})\|_{W_{\#}^{1,2}} \leq \frac{\eta}{4 \sin^2(\theta/2)} \frac{\|\nabla \Phi_0\|_{\infty}}{\mu C_{\mathbb{E}}^1}.$$

and thus maps continuously the following ball of $L_{\#}^2(\Gamma_0, \mathbb{R}^2)$:

$$B = \left\{ \mathbf{u} \in L_{\#}^2 \mid \|\mathbf{u}\|_{L^2} \leq \frac{\eta}{4 \sin^2(\theta/2)} \frac{\|\nabla \Phi_0\|_{\infty}}{\mu C_{\mathbb{E}}^0} \right\}.$$

Then, because the injection $W_{\#}^{1,2} \hookrightarrow L_{\#}^2$ is compact, we can apply Schauder's fixed point theorem (see e.g. Theorem 9.12-1 in [13]) to obtain the existence of at least one fixed point of the mapping \mathcal{H} , which is a solution to (4.27). The bound (4.28) of (a) follows from (4.33).

Furthermore, \mathcal{H} satisfies the Lipschitz bound:

$$\|\mathcal{H}(\mathbf{u}) - \mathcal{H}(\mathbf{u}')\|_{L^2} \leq \frac{\eta}{4 \sin^2(\theta/2)} \frac{2\|\nabla^2 \Phi_0\|_{\infty}}{\mu C_{\mathbb{E}}^1} \|\mathbf{u} - \mathbf{u}'\|_{L^2}.$$

Thus we may apply the Banach fixed point theorem (see e.g. Theorem 3.7-1 in [13]) to show there exists a unique fixed point to \mathcal{H} under the condition:

$$\frac{\eta}{4 \sin^2(\theta/2)} < \frac{\mu C_{\mathbb{E}}^1}{2\|\nabla^2 \Phi_0\|_{\infty}}.$$

Since $4 \sin^2(\theta/2) \leq \theta^2$, this proves (b).

Finally, assume that Φ_0 is smooth and $\mathbf{u}^c \in W_{\#}^{1,2}$ is a solution of the Euler-Lagrange system (4.27). The finite difference technique for elliptic regularity (see e.g. [18], Section 6.3.1) ensures that $\mathbf{u}^c \in W_{\#}^{k,2}$ for any $k \geq 2$. Let us show the bound (4.30) by recursion. Set:

$$\mathbf{g} = \mathbf{F}_{\theta}(\mathbf{x}, 2\mathbf{u}^c).$$

For $k = 2$, we test (4.31) with $\mathbf{v}' = \partial_{\gamma} \mathbf{v}$ for some $\mathbf{v} \in C^{\infty}(\Gamma_0, \mathbb{R}^2)$ and $\ell = 1, 2$. Then

$$\begin{aligned} \frac{\eta}{4 \sin^2(\theta/2)} \int_{\Gamma_0} \mathbf{g} \cdot \partial_{\ell} \mathbf{v} &= \int_{\Gamma_0} \lambda \operatorname{div}(\mathbf{u}) \operatorname{div}(\partial_{\ell} \mathbf{v}) + 2\mu \varepsilon(\mathbf{u}) : \varepsilon(\partial_{\ell} \mathbf{v}) \\ &= - \int_{\Gamma_0} \lambda \operatorname{div}(\partial_{\ell} \mathbf{u}) \operatorname{div}(\mathbf{v}) + 2\mu \varepsilon(\partial_{\ell} \mathbf{u}) : \varepsilon(\mathbf{v}), \end{aligned}$$

which implies that $\mu \|\nabla \partial_{\ell} \mathbf{u}\|_{L^2} \leq \frac{\eta}{4 \sin^2(\theta/2)} \|\mathbf{g}\|_{L^2} \leq \frac{\eta}{4 \sin^2(\theta/2)} \|\nabla \Phi_0\|_{L^{\infty}}$ and thanks to (4.28):

$$\|\mathbf{u}\|_{2,2} \leq \frac{C_2 \eta}{4 \sin^2(\theta/2)},$$

where the constant C_2 depends only on \mathbb{E} , μ and $\|\Phi_0\|_{C^1(\Gamma_0)}$. Next, for $k \geq 3$ we use the test function $\Delta^k \mathbf{u}^c$ and the Fourier transform:

$$\begin{aligned} \sum_{\mathbf{k} \in \mathcal{R}_0^* \setminus \{0\}} (2\pi)^2 |2\pi \mathbf{k}|^{2k} \left(2\mu \left| \frac{\mathbf{k} \otimes \mathbf{u}_{\mathbf{k}}^c + \mathbf{u}^c \otimes \mathbf{k}}{2} \right|^2 + \lambda |\mathbf{k} \cdot \mathbf{u}_{\mathbf{k}}^c|^2 \right) \\ = \frac{\eta}{4 \sin^2(\theta/2)} \sum_{\mathbf{k} \in \mathcal{R}_0^* \setminus \{0\}} |2\pi \mathbf{k}|^{2k} \overline{\mathbf{u}_{\mathbf{k}}^c} \cdot \mathbf{g}_{\mathbf{k}}, \end{aligned}$$

and therefore by the Cauchy-Schartz inequality,

$$\begin{aligned} \mu \sum_{\mathbf{k} \in \mathcal{R}_0^* \setminus \{\mathbf{0}\}} |2\pi\mathbf{k}|^{2k+2} |\mathbf{u}_{\mathbf{k}}^c|^2 &\leq \frac{\eta}{4 \sin^2(\theta/2)} \sum_{\mathbf{k} \in \mathcal{R}_0^* \setminus \{\mathbf{0}\}} (|2\pi\mathbf{k}|^k |\mathbf{u}_{\mathbf{k}}|) (|2\pi\mathbf{k}|^k |\mathbf{g}_{\mathbf{k}}|) \\ &\leq \frac{\eta}{4 \sin^2(\theta/2)} \left(\sum_{\mathbf{k} \in \mathcal{R}_0^* \setminus \{\mathbf{0}\}} |2\pi\mathbf{k}|^{2k} |\mathbf{u}_{\mathbf{k}}|^2 \right)^{1/2} \left(\sum_{\mathbf{k} \in \mathcal{R}_0^* \setminus \{\mathbf{0}\}} |2\pi\mathbf{k}|^{2k} |\mathbf{g}_{\mathbf{k}}|^2 \right)^{1/2}. \end{aligned}$$

Thus $\mu \|\nabla^{k+1} \mathbf{u}^c\|_{L^2}^2 \leq \frac{\eta}{4 \sin^2(\theta/2)} \|\nabla^k \mathbf{u}^c\|_{L^2} \|\nabla^k \mathbf{g}\|_{L^2}$. Now, by an appropriate Faà di Bruno's formula we can show that there exists a generic constant $C \geq 0$ independent of η and θ such that: $\|\nabla^k \mathbf{g}\|_{L^2} \leq C \|\Phi_0\|_{C^{k+1}} \|\mathbf{u}^c\|_{k,2}$, and thus

$$\|\nabla^{k+1} \mathbf{u}^c\|_{L^2} \leq \left(\frac{\eta}{4 \sin^2(\theta/2)} \frac{C \|\Phi_0\|_{C^{k+1}}}{\mu} \right)^{1/2} \|\mathbf{u}^c\|_{k,2}.$$

Let us now assume that for $k \geq 2$,

$$\|\mathbf{u}\|_{k,2} \leq C_k \frac{\eta^{k/2}}{4 \sin^k(\theta/2)},$$

where the constant C_k depends only on E , μ and $\|\Phi_0\|_{C^1(\Gamma_0)}$. Note that this is already true for $k = 2$. Then we have shown that

$$\begin{aligned} \|\mathbf{u}\|_{k+1,2} = \|\mathbf{u}\|_{k,2} + \|\nabla^{k+1} \mathbf{u}^c\|_{L^2}^2 &\leq \left(\frac{\eta}{4 \sin^2(\theta/2)} \frac{C \|\Phi_0\|_{C^{k+1}}}{\mu} \right)^{1/2} C_k \frac{\eta^{k/2}}{4 \sin^k(\theta/2)} \\ &\leq C_{k+1} \frac{\eta^{k+1/2}}{4 \sin^{k+1}(\theta/2)}, \end{aligned}$$

where $C_{k+1} = C_k \left(\frac{C \|\Phi_0\|_{C^{k+1}}}{\mu} \right)^{1/2}$. Proceeding inductively, we have shown (c). \square

5. Numerical study: example of graphene bilayers. As an illustration of the previous framework and analysis, we propose to study numerically the relaxation of a slightly twisted graphene bilayer system [16]. This particular assembly is also known for its exceptional electronic properties [7–9] which might be influenced by the domain formation due to mechanical relaxation.

Parameters. Graphene corresponds to a triangular lattice structure with the basis

$$\mathbf{E} = \sqrt{3}a_0 \begin{bmatrix} \sqrt{3}/2 & \sqrt{3}/2 \\ -1/2 & 1/2 \end{bmatrix} \quad \text{where } a_0 = 1.42 \text{ nm},$$

such that the twisted lattices are given by (4.21). The inter-layer GSFE is assumed to take the form [10]:

$$(5.1) \quad \Phi_{1+}^{\text{misfit}}(\gamma_2) = \phi(2\pi\mathbf{E}_2^{-1}\gamma_2), \quad \Phi_{2-}^{\text{misfit}}(\gamma_1) = \phi(2\pi\mathbf{E}_1^{-1}\gamma_1),$$

where the symmetry-adapted functional ϕ is defined periodically on $[0, 2\pi)^2$ as:

$$\begin{aligned} \phi \left(\begin{bmatrix} v \\ w \end{bmatrix} \right) &:= c_0 + c_1 [\cos(v) + \cos(w) + \cos(v+w)] \\ &\quad + c_2 [\cos(v+2w) + \cos(v-w) + \cos(2v+w)] \\ &\quad + c_3 [\cos(2v) + \cos(2w) + \cos(2v+2w)]. \end{aligned}$$

The Lamé parameters λ , μ (4.20) of the graphene sheets as well as the GSFE coefficients c_{0-3} accurately fitted from vdW-DFT calculations [10] are summed up in Table 1.

λ	μ	c_0	c_1	c_2	c_3
37,950	47,352	6.832	4.064	-0.374	-0.095

Table 1: Elastic moduli and GSFE coefficients for graphene bilayers in units of meV/unit cell area.

Discretization and numerical scheme. For consistency, we discretize here directly the minimization problem (3.21). Let us define a uniform $N \times N$ grid on the torus $[-1/2, 1/2]^2$:

$$(5.2) \quad \mathcal{G}_N := \left\{ \frac{\delta - \lfloor N/2 \rfloor}{N}, \dots, \frac{-1}{N}, 0, \frac{1}{N}, \dots, \frac{\lfloor N/2 \rfloor}{N} \right\}^2, \quad \text{where } \delta = \begin{cases} 0, & N \text{ odd,} \\ 1, & N \text{ even.} \end{cases}$$

We introduce next the set of unknown nodal values $\mathbf{U}^N = \{\mathbf{U}_{\mathbf{n}}^N\}_{\mathbf{n} \in \mathcal{G}_N}$ such that nodal values of the displacements \mathbf{u}_1 and \mathbf{u}_2 on Γ_2 and Γ_1 respectively are given by

$$\mathbf{u}_1^N(\mathbf{E}_2 \mathbf{n}) = \mathbf{U}_{\mathbf{n}}^N = -\mathbf{u}_2^N(-\mathbf{E}_1 \mathbf{n}) \quad \text{for } \mathbf{n} \in \mathcal{G}_N,$$

where we have used the symmetry (4.27) to reduce the number of free variables. We next interpolate these values by the Fourier series:

$$(5.3) \quad \mathbf{u}_1^N(\boldsymbol{\gamma}_2) = \sum_{\mathbf{k} \in \mathcal{G}_N} \hat{\mathbf{U}}_{\mathbf{k}}^N e^{\frac{2i\pi}{N} \mathbf{k} \cdot \mathbf{E}_2^{-1} \boldsymbol{\gamma}_2}, \quad \mathbf{u}_2^N(\boldsymbol{\gamma}_1) = - \sum_{\mathbf{k} \in \mathcal{G}_N} \hat{\mathbf{U}}_{\mathbf{k}}^N e^{-\frac{2i\pi}{N} \mathbf{k} \cdot \mathbf{E}_1^{-1} \boldsymbol{\gamma}_1}.$$

Note that the Fourier coefficients appearing in this expression can be computed efficiently from the nodal values \mathbf{U}^N by the Fast Fourier Transform. The elastic energy (4.20) is then exactly computable, while the misfit energy (3.20) can be approximated by uniform quadrature, a straightforward calculation leading to:

$$(5.4) \quad E_N^{\text{misfit}}(\mathbf{U}) := \frac{1}{2N^2} \sum_{\mathbf{n} \in \mathcal{G}_N} [\phi(2\pi(\mathbf{n} - 2\mathbf{E}_2^{-1} \mathbf{U}_{\mathbf{n}}^N)) + \phi(2\pi(\mathbf{n} - 2\mathbf{E}_1^{-1} \mathbf{U}_{\mathbf{n}}^N))].$$

An explicit expression can also be obtained for the gradient of these energies. We implemented this approach in the Julia language [4], using the limited-memory BFGS quasi-Newton algorithm from the `Optim.jl` Julia library to minimize numerically the resulting total energy.

Results and Discussion. We first discuss numerical results obtained for the twist angle $\theta = 0.3^\circ$, presented in Figure 4. The grid size is chosen as $N = 144$. We observe the formation of a well-defined triangular pattern in configuration space, see Figure 4(b). In real space, this corresponds to the triangular meso-scale pattern observed in experiments results [33]: relaxation causes the expansion of the regions of lowest-energy stacking, where the lattices are staggered (graphite or Bernal stacking), into well-defined triangular domains arranged in a hexagonal pattern, and the contraction of higher-energy stacking regions, in particular where lattices are vertically aligned. Note that expansion or contraction in configuration space (as seen on Figure 4(c)) corresponds to a rotation in real space (as seen on Figure 4(d)), such that the effective local twist angle is enhanced in regions of higher energy and reduced in regions of lower energy. Thus, the layers are brought into almost perfect alignment with the AB/BA triangular domains.

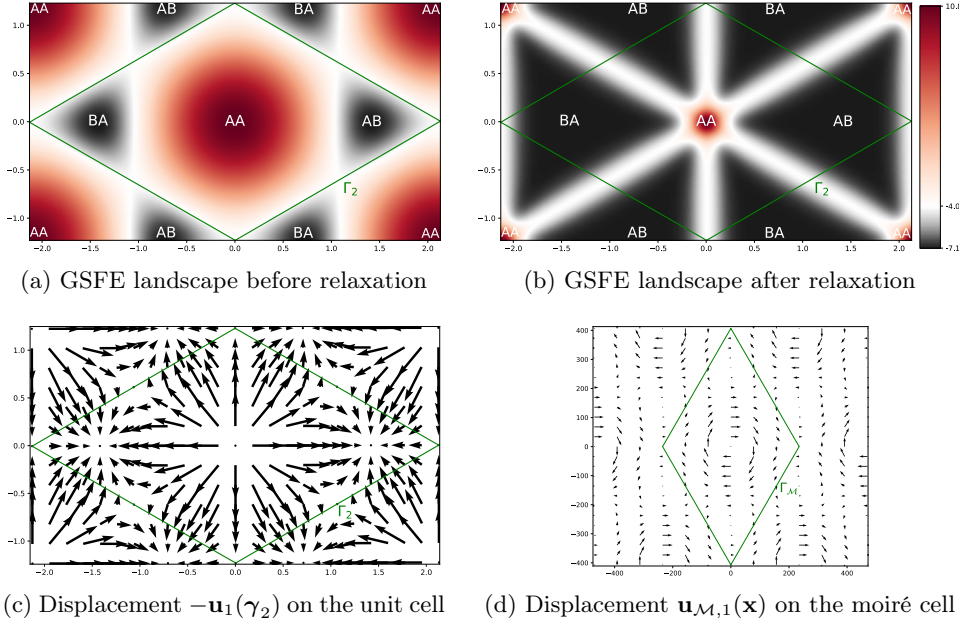


Fig. 4: Relaxation for a graphene bilayer with a 0.3° relative twist angle. (a): GSFE functional Φ_{1+} in the reference configuration space Γ_2 , showing the maxima and minima at shifts corresponding respectively to AA and AB/BA stackings. (b) Relaxed local misfit energy as a function of original shift, $\Phi_{1+}(\gamma_2 - 2\mathbf{u}_1(\gamma_2))$. (c) Displacement of atoms in layer 1 in configuration space $-\mathbf{u}_1$, corresponding to the change in the local stacking configuration if layer 2 were not moving. (d) Displacement field of atoms in layer 1 in real space, with the periodicity of the moiré cell.

Next, let us discuss briefly the atomistic mappings corresponding to the deformations computed above. To account for the hexagonal (multilattice) nature of the graphene lattice, two sublattices denoted by A, B can be introduced with respective shifts $\mp a_0/2\mathbf{e}_1$ in each of the layers before the twist is taken into account. We then make the simplification that the shift field [30] is fixed: for each of the two layers, the deformed sublattices from a starting configuration $\omega = (\gamma_1, \gamma_2)$ are given by the atomistic deformations:

$$\begin{cases} \mathbf{Y}_{1,A}^\omega(\mathbf{r}_1) = \mathbf{r}_1 - a_0/2\mathbf{R}_{-\theta/2}\mathbf{e}_1 + \mathbf{u}_1(\gamma_2 - \mathbf{r}_1), \\ \mathbf{Y}_{1,B}^\omega(\mathbf{r}_1) = \mathbf{r}_1 + a_0/2\mathbf{R}_{-\theta/2}\mathbf{e}_1 + \mathbf{u}_1(\gamma_2 - \mathbf{r}_1), \end{cases} \quad \text{for } \mathbf{r}_1 \in \gamma_1 + \mathcal{R}_1,$$

$$\begin{cases} \mathbf{Y}_{2,A}^\omega(\mathbf{r}_2) = \mathbf{r}_2 - a_0/2\mathbf{R}_{+\theta/2}\mathbf{e}_1 + \mathbf{u}_2(\gamma_1 - \mathbf{r}_2), \\ \mathbf{Y}_{2,B}^\omega(\mathbf{r}_2) = \mathbf{r}_2 + a_0/2\mathbf{R}_{+\theta/2}\mathbf{e}_1 + \mathbf{u}_2(\gamma_1 - \mathbf{r}_2), \end{cases} \quad \text{for } \mathbf{r}_2 \in \gamma_2 + \mathcal{R}_2.$$

These mappings allow us to visualize the domain structures at the atomistic level in real space, as presented in Figure 1 for a 3° twist angle².

²Note that interlayer coupling used in the computation leading to Figure 1 was artificially enhanced by a factor of 100 with respect to the coefficients in 1 such that the scales of both unit and moiré cells are visible while still ensuring significant relaxation.

A closer inspection of these structures reveals that the pattern is *not periodic* with the moiré lattice $\Gamma_{\mathcal{M}}$, although the calculation of the hull functions \mathbf{u}_1 and \mathbf{u}_2 uses periodic boundary conditions, and the moiré cell $\Gamma_{\mathcal{M}}$ introduced in paragraph 4.1 resembles a real-space supercell. In this sense, our method allows us to truly model the incommensurability of the lattices \mathcal{R}_1 and \mathcal{R}_2 without the need for constructing an appropriate supercell as in previous works [16, 31, 34, 35].

Acknowledgments. This work was supported in part by ARO MURI Award W911NF-14-1-0247.

Appendix A. Proof of Prop. 2.8. In this appendix, we detail the technical proof of Proposition 2.8, which we recall first for ease of reading.

PROPOSITION A.1.

$$(A.1) \quad \|\hat{\mathbf{u}}_j - \tilde{\mathbf{u}}_j\|_{L^q(\Omega)} \leq \left(\frac{|\Gamma_j|}{2q+1} \right)^{1/q} \theta^2 \|\nabla_{\omega}^2 \mathbf{u}_j\|_{L^q(X_j)}$$

where $X_j = \times_{i \neq j} \Gamma_i$ is the subset of the transversal corresponding to lattice sites of layer j , $\nabla_{\omega}^2 \mathbf{u}_j$ is understood as a 2-linear form for which the norm is defined as $\|\ell\| := \sup_{|\mathbf{h}_1|=|\mathbf{h}_2|=1} |\ell[\mathbf{h}_1, \mathbf{h}_2]|$ and

$$(A.2) \quad \theta = \sqrt{p} \sup_{1 \leq i, j \leq p} \|\mathbf{E}_i - \mathbf{E}_j\|, \quad \text{where } \|\cdot\| \text{ denotes the } \mathbb{R}^2\text{-operator norm.}$$

Proof. It is natural to relate this result to local finite element interpolant error estimation and follow similar steps. Let $\omega \in \Omega$ be an arbitrary configuration, j be an arbitrary layer number. Consider a Taylor expansion up to degree 1 of \mathbf{u}_j around the point $\Pi_j \omega$:

$$T_{\omega}^1 \mathbf{u}_j(\delta\omega) = \mathbf{u}_j(\Pi_j \omega) + \nabla_{\omega} \mathbf{u}_j(\Pi_j \omega) \cdot \delta\omega \text{ where } \delta\omega = (\delta\omega_1, \dots, \delta\omega_p) \in \mathbb{R}^{2p}, \delta\omega_j = \mathbf{0}.$$

Using the integral formula for the residual of the Taylor series, we have:

$$\begin{aligned} \mathbf{u}_j(\Pi_j \omega + \delta\omega) - T_{\omega}^1 \mathbf{u}_j(\delta\omega) &= \int_0^1 \frac{(1-h)^2}{2} \frac{d^2 \mathbf{u}_j}{dh^2}(\Pi_j \omega + h\delta\omega) dh \\ &= \int_0^1 \frac{(1-h)^2}{2} \nabla_{\omega}^2 \mathbf{u}_j(\Pi_j \omega + h\delta\omega) [\delta\omega, \delta\omega] dh, \end{aligned}$$

so by Jensen's inequality we obtain the estimate:

$$(A.3) \quad \|\mathbf{u}_j(\Pi_j \omega + \delta\omega) - T_{\omega}^1 \mathbf{u}_j(\delta\omega)\|^q \leq \|\delta\omega\|^{2q} \int_0^1 \frac{(1-h)^{2q}}{2^q} \|\nabla_{\omega}^2 \mathbf{u}_j(\Pi_j \omega + h\delta\omega)\|^q dh.$$

As earlier (see (2.10)), let us write $\gamma_j = \mathbf{E}_j \begin{bmatrix} s \\ t \end{bmatrix}$ with $0 \leq s, t < 1$. The lattice sites in layer j around the origin are located at the four points \mathbf{r}_{ab} with $a, b \in \{0, 1\}$ defined as in (2.6). One checks easily from the definition (2.12) that

$$\mathbf{T}_{-\mathbf{r}_{ab}} \omega = \Pi_j \omega + \delta\omega_{ab} \quad \text{for } a, b \in \{0, 1\},$$

where the shifts $\delta\omega_{00}, \delta\omega_{10}, \delta\omega_{01}, \delta\omega_{11}$ can be chosen as

$$\begin{aligned}\delta\omega_{00} &= \left((\mathbf{E}_1 - \mathbf{E}_j) \begin{bmatrix} s \\ t \end{bmatrix}, \dots, (\mathbf{E}_p - \mathbf{E}_j) \begin{bmatrix} s \\ t \end{bmatrix} \right), \\ \delta\omega_{10} &= \left((\mathbf{E}_1 - \mathbf{E}_j) \begin{bmatrix} s-1 \\ t \end{bmatrix}, \dots, (\mathbf{E}_p - \mathbf{E}_j) \begin{bmatrix} s-1 \\ t \end{bmatrix} \right), \\ \delta\omega_{01} &= \left((\mathbf{E}_1 - \mathbf{E}_j) \begin{bmatrix} s \\ t-1 \end{bmatrix}, \dots, (\mathbf{E}_p - \mathbf{E}_j) \begin{bmatrix} s \\ t-1 \end{bmatrix} \right), \\ \delta\omega_{11} &= \left((\mathbf{E}_1 - \mathbf{E}_j) \begin{bmatrix} s-1 \\ t-1 \end{bmatrix}, \dots, (\mathbf{E}_p - \mathbf{E}_j) \begin{bmatrix} s-1 \\ t-1 \end{bmatrix} \right)\end{aligned}$$

since $\delta\omega_{ab}$ is defined on Ω and is thus invariant under lattice shifts. Note that for $a, b \in \{0, 1\}$,

$$\delta\omega_{ab,j} = \mathbf{0} \quad \text{and} \quad \|\delta\omega_{ab}\| \leq \sqrt{2} \theta,$$

where θ is defined in (2.14). Furthermore, the weighted average of these shifts is zero:

$$\sum_{a,b \in \{0,1\}} \alpha_{ab} \delta\omega_{ab} = 0,$$

where we have introduced the bilinear weights

$$\alpha_{00} = (1-s)(1-t), \quad \alpha_{10} = s(1-t), \quad \alpha_{01} = (1-s)t, \quad \alpha_{11} = st.$$

As a consequence, by the affine character of the Taylor approximant $T_\omega^1 \mathbf{u}_j$ defined above,

$$(A.4) \quad \hat{\mathbf{u}}_j(\omega) = T_\omega^1 \mathbf{u}_j(0) = \sum_{a,b \in \{0,1\}} \alpha_{ab} T_\omega^1 \mathbf{u}_j(\delta\omega_{ab}).$$

Let us now rewrite the definition (2.10) of the bilinear interpolant $\tilde{\mathbf{u}}_j$ as:

$$(A.5) \quad \tilde{\mathbf{u}}_j(\omega) = \sum_{a,b \in \{0,1\}} \alpha_{ab} \mathbf{u}_j(\Pi_j \omega + \delta\omega_{ab}).$$

Taking the difference of the identities (A.4), (A.5) and using convexity of the norm and the above Taylor estimate (A.3), we find the pointwise estimate

$$\|\hat{\mathbf{u}}_j(\omega) - \tilde{\mathbf{u}}_j(\omega)\|^q \leq \theta^{2q} \int_0^1 (1-h)^{2q} \sum_{a,b \in \{0,1\}} \alpha_{ab} \|\nabla_\omega^2 \mathbf{u}_j(\Pi_j \omega + h\delta\omega_{ab})\|^q dh.$$

We may now integrate over the configuration parameter $\omega = (\gamma_1, \dots, \gamma_p)$. The difference between ω and $(\Pi_j \omega + h\delta\omega_{ab})$ depends only on s, t and h , for example

$$\omega - (\Pi_j \omega + h\delta\omega_{00}) = - \left((h\mathbf{E}_j + (1-h)\mathbf{E}_1) \begin{bmatrix} s \\ t \end{bmatrix}, \dots, (h\mathbf{E}_j + (1-h)\mathbf{E}_p) \begin{bmatrix} s \\ t \end{bmatrix} \right).$$

Integrating over the variables γ_i for $i \neq j$ with fixed values of $\gamma_j = \mathbf{E}_j \begin{bmatrix} s \\ t \end{bmatrix}$ and h we find that by translation invariance of the Lebesgue measure,

$$\int \cdots \int_{\times_{i \neq j} \Gamma_i} \|\nabla_\omega^2 \mathbf{u}_j(\Pi_j \omega + h\delta\omega_{ab})\|_{\text{op}}^q \prod_{i \neq j} d\gamma_i = \|\nabla_\omega^2 \mathbf{u}_j\|_{L^q(X_j, \|\cdot\|_{\text{op}})}^q.$$

This leads to

$$\int \cdots \int_{\times_{i \neq j} \Gamma_i} \|\hat{\mathbf{u}}_j(\omega) - \tilde{\mathbf{u}}_j(\omega)\|^q \prod_{i \neq j} d\gamma_i \leq \theta^{2q} \|\nabla_{\omega}^2 \mathbf{u}_j\|_{L^q(X_j, \|\cdot\|_{\text{op}})} \int_0^1 (1-h)^{2q} dh.$$

Since the right-hand side does not depend on the remaining variable γ_j , one last integration over it yields:

$$\|\hat{\mathbf{u}}_j(\omega) - \tilde{\mathbf{u}}_j(\omega)\|_{L^q(\Omega)}^q \leq \frac{|\Gamma_j|}{2q+1} \theta^{2q} \|\nabla_{\omega}^2 \mathbf{u}_j\|_{L^q(X_j, \|\cdot\|_{\text{op}})}^q,$$

which proves the desired estimate (2.13). \square

REFERENCES

- [1] S. AUBRY AND P. LE DAERON, *The discrete Frenkel-Kontorova model and its extensions. I. Exact results for the ground-states*, Physica D, 8 (1983), pp. 381–422.
- [2] J. BELLISSARD, *Coherent and dissipative transport in aperiodic solids*, in Lecture Notes in Physics, vol. 597, Springer, 2003, pp. 413–486.
- [3] J. BELLISSARD, A. VAN ELST, AND H. SCHULZ-BALDES, *The noncommutative geometry of the quantum Hall effect*, Journal of Mathematical Physics, 35 (1994), pp. 5373–5451.
- [4] J. BEZANSON, A. EDELMAN, S. KARPINSKI, AND V. B. SHAH, *Julia: A fresh approach to numerical computing*, SIAM review, 59 (2017), pp. 65–98.
- [5] X. BLANC, C. LE BRIS, AND P.-L. LIONS, *Atomistic to continuum limits for computational materials science*, ESAIM: Mathematical Modelling and Numerical Analysis, 41 (2007), pp. 391–426.
- [6] E. CANCÈS, P. CAZEAUX, AND M. LUSKIN, *Generalized Kubo formulas for the transport properties of incommensurate 2D atomic heterostructures*, Journal of Mathematical Physics, 58 (2017), p. 063502.
- [7] Y. CAO, V. FATEMI, A. DEMIR, S. FANG, S. L. TOMARKEK, J. Y. LUO, J. D. SANCHEZ-YAMAGISHI, K. WATANABE, T. TANIGUCHI, E. KAXIRAS, AND P. JARILLO-HERRERO, *Correlated insulator behaviour at half-filling in magic-angle graphene superlattices*, Nature, 556 (2018), pp. 80–84.
- [8] Y. CAO, V. FATEMI, S. FANG, K. WATANABE, T. TANIGUCHI, E. KAXIRAS, AND P. JARILLO-HERRERO, *Unconventional superconductivity in magic-angle graphene superlattices*, Nature, 556 (2018), pp. 43–50.
- [9] S. CARR, D. MASSATT, S. FANG, P. CAZEAUX, M. LUSKIN, AND E. KAXIRAS, *Twistronics: Manipulating the electronic properties of two-dimensional layered structures through their twist angle*, Physical Review B, 95 (2017), p. 075420, <http://dx.doi.org/10.1103/PhysRevB.95.075420>.
- [10] S. CARR, D. MASSATT, S. B. TORRISI, P. CAZEAUX, M. LUSKIN, AND E. KAXIRAS, *Relaxation and Domain Formation in Incommensurate 2D Heterostructures*. arXiv preprint arXiv:1805.06972, 2018.
- [11] A. H. CASTRO NETO, F. GUINEA, N. M. R. PERES, K. S. NOVOSELOV, AND A. K. GEIM, *The electronic properties of graphene*, Reviews of Modern Physics, 81 (2009), p. 109.
- [12] P. CAZEAUX, M. LUSKIN, AND E. B. TADMOR, *Analysis of rippling in incommensurate one-dimensional coupled chains*, Multiscale Modeling & Simulation, 15 (2017), pp. 56–73.
- [13] P. G. CIARLET, *Linear and nonlinear functional analysis with applications*, vol. 130, Siam, 2013.
- [14] G. CONSTANTINESCU, A. KUC, AND T. HEINE, *Stacking in bulk and bilayer hexagonal boron nitride*, Physical review letters, 111 (2013), p. 036104.
- [15] B. DACOROGNA, *Direct methods in the calculus of variations*, vol. 78, Springer Science & Business Media, 2007.
- [16] S. DAI, Y. XIANG, AND D. J. SROLOVITZ, *Twisted bilayer graphene: Moiré with a twist*, Nano Letters, 16 (2016), pp. 5923–5927, <http://dx.doi.org/10.1021/acs.nanolett.6b02870>.
- [17] M. I. ESPAÑOL, D. GOLOVATY, AND J. P. WILBER, *Discrete-to-continuum modelling of weakly interacting incommensurate two-dimensional lattices*, Proceedings of the Royal Society of London A: Mathematical, Physical and Engineering Sciences, 474 (2018).
- [18] L. C. EVANS, *Partial Differential Equations: Second Edition*, Springer series in computational physics, American Mathematical Society, Providence, Rhode Island, 2010.

- [19] A. K. GEIM AND I. V. GRIGORIEVA, *Van der Waals heterostructures*, Nature, 499 (2013), pp. 419–425.
- [20] X. GONG AND E. MELE, *Stacking textures and singularities in bilayer graphene*, Physical Review B, 89 (2014), p. 121415.
- [21] K. KIM, A. DASILVA, S. HUANG, B. FALLAHAZAD, S. LARENTIS, T. TANIGUCHI, K. WATANABE, B. J. LEROY, A. H. MACDONALD, AND E. TUTUC, *Tunable moiré bands and strong correlations in small-twist-angle bilayer graphene*, Proceedings of the National Academy of Sciences, 114 (2017), pp. 3364–3369.
- [22] A. N. KOLMOGOROV AND V. H. CRESPI, *Smoothest bearings: interlayer sliding in multiwalled carbon nanotubes*, Physical Review Letters, 85 (2000), p. 4727.
- [23] J. M. B. LOPES DOS SANTOS, N. M. R. PERES, AND A. H. CASTRO NETO, *Graphene bilayer with a twist: Electronic structure*, Physical Review Letters, 99 (2007), p. 256802.
- [24] N. MAROM, J. BERNSTEIN, J. GAREL, A. TKATCHENKO, E. JOSELEVICH, L. KRONIK, AND O. HOD, *Stacking and registry effects in layered materials: the case of hexagonal boron nitride*, Physical Review Letters, 105 (2010), p. 046801.
- [25] D. MASSATT, M. LUSKIN, AND C. ORTNER, *Electronic density of states for incommensurate layers*, Multiscale Modeling & Simulation, 15 (2017), pp. 476–499.
- [26] K. S. NOVOSELOV, A. K. GEIM, S. V. MOROZOV, D. JIANG, Y. ZHANG, S. V. DUBONOS, I. V. GRIGORIEVA, AND A. A. FIRSOV, *Electric field effect in atomically thin carbon films*, Science, 306 (2004), pp. 666–669.
- [27] C. ORTNER AND F. THEIL, *Justification of the Cauchy–Born approximation of elastodynamics*, Archive for Rational Mechanics and Analysis, 207 (2013), pp. 1025–1073.
- [28] E. PRODAN, *Quantum transport in disordered systems under magnetic fields: A study based on operator algebras*, Applied Mathematics Research eXpress, 2013 (2013), pp. 176–265, <http://dx.doi.org/10.1093/amrx/abs017>.
- [29] G. A. TRITSARIS, S. N. SHIRODKAR, E. KAXIRAS, P. CAZEAUX, M. LUSKIN, P. PLECHÁČ, AND E. CANCÈS, *Perturbation theory for weakly coupled two-dimensional layers*, Journal of Materials Research, 31 (2016), pp. 959–966, <http://dx.doi.org/10.1557/jmr.2016.99>, http://journals.cambridge.org/article_S0884291416000996.
- [30] B. VAN KOTEN AND C. ORTNER, *Symmetries of 2-lattices and second order accuracy of the Cauchy–Born model*, Multiscale Modeling & Simulation, 11 (2013), pp. 615–634.
- [31] M. M. VAN WIJK, A. SCHURING, M. I. KATSNELSON, AND A. FASOLINO, *Relaxation of moiré patterns for slightly misaligned identical lattices: graphene on graphite*, 2D Materials, 2 (2015), p. 034010.
- [32] V. VITEK, *Intrinsic stacking faults in body-centred cubic crystals*, Philosophical Magazine, 18 (1968), pp. 773–786.
- [33] H. YOO, K. ZHANG, R. ENGELKE, P. CAZEAUX, S. SUNG, R. HOVDEN, A. W. TSEN, T. TANIGUCHI, K. WATANABE, G.-C. YI, M. KIM, M. LUSKIN, E. TADMOR, AND P. KIM, *Atomic reconstruction at van der waals interface in twisted bilayer graphene*. arXiv preprint arXiv:1804.03806, 2018.
- [34] K. ZHANG AND E. B. TADMOR, *Structural and electron diffraction scaling of twisted graphene bilayers*, Journal of the Mechanics and Physics of Solids, 112 (2017).
- [35] K. ZHANG AND E. B. TADMOR, *Energy and moiré patterns in 2D bilayers in translation and rotation: A study using an efficient discrete–continuum interlayer potential*, Extreme Mechanics Letters, 14 (2017), pp. 16–22.
- [36] S. ZHOU, J. HAN, S. DAI, J. SUN, AND D. J. SROLOVITZ, *Van der Waals bilayer energetics: Generalized stacking-fault energy of graphene, boron nitride, and graphene/boron nitride bilayers*, Physical Review B, 92 (2015), p. 155438.